

Primordial black holes and curvature perturbations from false vacuum islands

Rong-Gen Cai,^{1,2,*} Yu-Shi Hao,^{2,3,†} and Shao-Jiang Wang^{2,4,‡}

¹*School of Physical Science and Technology, Ningbo University, Ningbo, 315211, China*

²*CAS Key Laboratory of Theoretical Physics, Institute of Theoretical Physics, Chinese Academy of Sciences (CAS), Beijing 100190, China*

³*School of Physical Sciences, University of Chinese Academy of Sciences (UCAS), Beijing 100049, China*

⁴*Asia Pacific Center for Theoretical Physics (APCTP), Pohang 37673, Korea*

Recently, much attention has been focused on the false vacuum islands that are flooded by an expanding ocean of true-vacuum bubbles slightly later than most of the other parts of the world. These delayed decay regions will accumulate locally larger vacuum energy density by staying in the false vacuum longer than those already transitioned into the true vacuum. A false vacuum island with thus acquired density contrast of a super-horizon size will evolve locally from radiation dominance to vacuum dominance, creating a local baby Universe that can be regarded effectively as a local closed Universe. If such density contrasts of super-horizon sizes can ever grow large enough to exceed the threshold of gravitational collapse, primordial black holes will form similar to those collapsing curvature perturbations on super-horizon scales induced by small-scale enhancements during inflation. If not, such density contrasts can still induce curvature perturbations potentially observable today. In this paper, we revisit and elaborate on the generations of primordial black holes and curvature perturbations from delayed-decayed false vacuum islands during asynchronous first-order phase transitions with fitting formulas convenient for future model-independent studies.

I. INTRODUCTION

The cosmological first-order phase transition (FOPT) [1–4] plays an essential role in probing the new physics [5, 6] beyond the standard model of particle physics in the early Universe via future detection of stochastic gravitational wave (GW) backgrounds [7–9] in the space-borne GW detectors like LISA [10–12] and Taiji [13–15] as well as TianQin [16–18]. Recently, there has been a renewed interest in generating primordial black holes (PBHs) from cosmological FOPTs via shrinking [19, 20] or accumulating [21] mechanisms other than early proposals of colliding mechanism [22–25] (see recent studies [26–29]).

The shrinking mechanism [19, 20] originated from the pictures of filtered dark matter [30] and Fermi-ball dark matter [31] during some specific FOPTs, where some particle species can acquire too large masses to barely penetrate the true-vacuum bubbles but are reflected and then trapped in the false vacuum phase, leading to direct formations of PBHs [19] or indirect PBH formations via collapsing Fermi balls [20]. Note that the reflected would-be massive particles in the filtered dark matter scenario can also annihilate to trigger baryogenesis [32, 33] instead of producing PBHs, and the Fermi-ball dark matter scenario can similarly produce baryon asymmetry via leptogenesis [34]. The direct shrinking mechanism [19] was further developed in Ref. [35] and exemplified for a PeV-scale model [36]. The indirect shrinking mechanism [20] was further elaborated on the population statistics [37] and its evolutionary endpoint [38] for the old phase remnants, and also exemplified for an electroweak model [39].

Correlated signals [40–46] were also proposed to discriminate different formation channels. Despite being highly model-dependent for both shrinking mechanisms, the direct shrinking mechanism was further criticized recently in Ref. [47] for the backreaction from trapped particles to reduce the compactness needed for PBH formations.

On the other hand, the accumulating mechanism [21] is model-independent, imposing no constraint on the properties of particles of phase transition models, but only takes advantage of inhomogeneous evolutions of asynchronous transition regions due to the stochastic nature of bubble nucleations. These delayed-decayed regions resemble and revive earlier proposals of trapped false vacuum domains [48–53]¹, and their subsequent PBH formations were further exemplified in the QCD-scale [55–58], electroweak-scale [59–63] and PeV-scale [64] models. More analytic estimations on the parameter dependence were carried out recently in Refs. [65–67] when these delayed-decayed false vacuum islands are approximated locally as exponentially expanding regions for an exponential nucleation rate [65, 66] or with a quadratic correction [67, 68]. In particular, different from earlier proposal [53] and its recent revisit [67] where only those pure false vacuum regions that never underwent single nucleation are supposed to collapse into PBHs [65], our accumulating mechanism [21] and its recent refinement [66] allows causal regions to collapse into PBHs even after they already started the process of nucleation as long as they started slightly late enough to accumulate sufficient local overdensities. Moreover, the recent refinement [66] fur-

* cairg@itp.ac.cn

† haoyushi@itp.ac.cn

‡ schwang@itp.ac.cn (corresponding author)

¹ See also a recent study [54] simulating the non-perturbative dynamics of single field inflation that might offer alternative channel for PBH formation from trapped false vacuum regions during inflation.

ther excludes bubble nucleations outside the postponed Hubble patches but inside the past light cone of final collapsed regions. Furthermore, another recent refinement [67] includes the bubble wall energy propagating into the postponed Hubble patch from those bubbles nucleated inside the past light cone of collapsed regions.

It is worth noting that a recent revisit [69] of our accumulating mechanism has cast doubt on the PBH formations from the critical collapse criteria, but proposed to form PBHs from the Schwarzschild criterion for the growing energy density of the domain walls separating between the delayed-decayed and normal-decayed regions. They pointed out that, as the relative difference in the red-shifted radiation densities generates a local overdensity, the delayed-decayed regions are still dominated by radiation energy density, providing only expansionary solutions instead of a contracting solution as realized in the usual inflationary PBH scenarios that induce a local curvature from the curvature perturbations. Here we take the chance to clarify our accumulating mechanism that, the local overdensities are gained, not through the relative difference in the red-shifted radiation energy densities, but from the undiluted false vacuum energy density (fixing the true vacuum at zero energy) in the delayed-decayed regions. These false vacuum islands would gradually be dominated by the false vacuum energy and expand locally faster than the outside regions, inflating into a local baby Universe [70] that can be treated effectively as a local closed Universe. Moreover, different from earlier proposals [48–53] that might lead to type II PBHs (see, for example, a recent study [71] and references therein), these delayed-decayed regions would not actually inflate into a detached baby Universe in the end due to subsequent bubble nucleations (see Fig. 1). Therefore, the original critical collapse criteria still apply in our case just as the usual inflationary PBH scenarios.

Even if the postponed overdensities never reach the critical threshold for the PBH formations, they can still induce potentially observable super-horizon curvature perturbations [72] at small scales, whose null detection imposes extremely strong constraints on the very-strong super-cooling slow-type FOPTs at low-energy scales. The same strategy for estimating the curvature perturbations also applies to the inhomogeneous distributions of spherical domain walls [73] and the inhomogeneous catalyzations of FOPTs from PBHs [74]. An alternative evaluation was presented in a recent study [75] for the curvature perturbations sourced from the isocurvature perturbations in the dark sector inherited from super-horizon fluctuations in the completion time of some low-scale dark-sector FOPT. Similar treatment can be found in a recent study [76] for a high-scale FOPT. In particular, the distribution of overdensities at given scales from different transition patches was found in a recent study [77] to be non-Gaussian, which merits further studies as this would significantly impact the PBH mass and abundance as well as the power spectrum of curvature perturbations.

In this paper, we revisit and elaborate on our accumulating mechanism for producing PBHs and curvature perturbations in the delayed-decayed regions during a general cosmological FOPT set up in Sec. II. In Sec. III, we solve for the evolution of these false vacuum islands by effectively transferring the inhomogeneities in the scale factors temporarily into the equation of state during the delayed-decayed process. In Sec. IV, we estimate numerically and fit analytically the PBH mass and abundance, but neglecting the effects from Refs. [66, 67] altogether for simplicity as the true-vacuum energy and bubble-wall energy propagating into the postponed Hubble patches from those bubbles nucleated inside the past light cone of collapsed regions have opposite effects on the growth of overdensities inside the postponed Hubble patches. In Sec. V, we directly compute the curvature perturbations by summing over all nucleation histories inside the postponed Hubble patches and truncating away the collapsed spacetime regions. The Sec. VI is devoted to the conclusion and discussion for future perspective.

II. GENERAL COSMOLOGICAL FOPTS

First, we set up the notations and conventions for a general cosmological FOPT. For a scalar field ϕ coupled to the background thermal plasma of temperature T with an effective potential $V_{\text{eff}}(\phi, T)$ admitting a false vacuum $V_+ \equiv V_{\text{eff}}(\phi_+)$ at ϕ_+ , there could develop a true vacuum $V_-(T) \equiv V_{\text{eff}}(\phi_-(T), T)$ at $\phi_-(T)$ with decreasing temperature T . We omit the minor temperature dependence in $\phi_-(T)$ as usually done for simplicity. Suppose the scalar field ϕ initially populates at ϕ_+ homogeneously over the space. In that case, the cosmological FOPT proceeds through random nucleations of true-vacuum bubbles in the false vacuum thermal background followed by rapid expansion until percolations via bubble collisions. The nucleation rate for a true-vacuum bubble per unit time and per unit volume is of an exponential form [78–81] $\Gamma(t) = A(t)e^{-B(t)} \equiv e^{-C(t)}$, where the pre-factor $A(t)$ accounts for quantum corrections of vacuum decay, and the bounce action $B(t)$ is evaluated from the Euclidean action at the bounce solution solved from the bounce equation given the boundary condition for describing a bubble of certain symmetry. In this paper, we study the usual case when $C(t)$ can be expanded linearly around some reference time t_0 as $C(t) = C(t_0) - \beta(t - t_0)$, in which case the nucleation rate can be approximated as $\Gamma(t) = e^{-C(t_0) + \beta(t - t_0)} = A(t_0)e^{-B(t_0) - \beta t_0} e^{\beta t} \equiv \Gamma_0 e^{\beta t}$ with $\beta = d \ln \Gamma / dt|_{t=t_0}$. In what follows, we will use the mass scale $\Gamma_0^{1/4}$ to normalize all dimensional quantities to be dimensionless, for example, $\bar{\beta} \equiv \beta / \Gamma_0^{1/4}$ and $\bar{t} \equiv \Gamma_0^{1/4} t$. The above bubble nucleation rate $\Gamma(t_{\text{nuc}}) = H(t_{\text{nuc}})^4$ defines a special moment t_{nuc} when balancing with the Hubble expansion rate $H(t_{\text{nuc}}) \equiv \dot{a}(t_{\text{nuc}})/a(t_{\text{nuc}}) \equiv H_{\text{nuc}}$, that is $\Gamma_0 e^{\beta t_{\text{nuc}}} = H_{\text{nuc}}^4$, which leads to a would-be useful approximation $\beta / H_{\text{nuc}} \approx 8W(\bar{\beta}/8)$ with the Lambert function defined by $z = W(z)e^{W(z)}$ after approximating

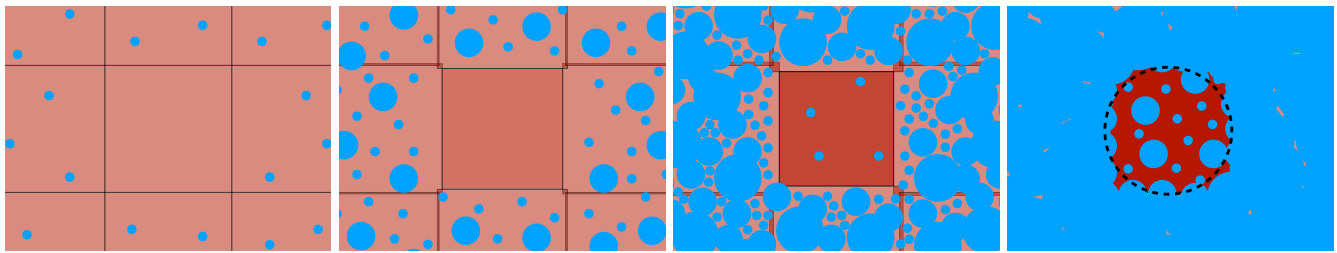


FIG. 1. A schematic illustration for the delayed-decayed false vacuum regions to accumulate (false) vacuum energy densities that gradually dominate the evolution of these overdensities, slightly shrinking the local comoving Hubble horizon that effectively induces local close patches. The subsequent bubble nucleations within these local baby Universes would prevent them from entering into a state of eternal inflation and hence being detached from our Universe, ensuring the conditions for PBH formations.

$H_{\text{nuc}} t_{\text{nuc}} \approx 1/2$ within the radiation dominance.

Next, we introduce the probability of staying at the false vacuum, which is equivalent to the volume fraction of false vacuum, $F(t) = \bar{V}_f(t)/\bar{V}$, defined by the ratio of the comoving volume of false vacuum $\bar{V}_f(t)$ out of a total comoving volume \bar{V} . Thus, the decrease of false vacuum volume $d\bar{V}_f(t)$ at t due to the volume increase at t from those bubbles nucleated at an earlier time t' reads

$$d\bar{V}_f(t) = - \int_{t_i}^t dN_b(t') \frac{\bar{V}_f(t)}{\bar{V}_f(t')} d\bar{V}_b(t; t'), \quad (1)$$

where the number of bubbles nucleated at t' within a time interval dt' is $dN_b(t') = \Gamma(t') V_f(t') dt'$ by definition as bubbles can only be nucleated within the physical false vacuum volume $V_f(t') = \bar{V}_f(t') a(t')^3$ with a scale factor $a(t')$, and the ratio $\bar{V}_f(t)/\bar{V}_f(t')$ simply takes into account the fact that only the parts of bubbles propagating into the false vacuum phase can decrease the false vacuum fraction [82, 83]. The increasing volume $d\bar{V}_b(t; t')$ from true-vacuum bubbles at t nucleated at an earlier time t' vanishes if $t = t'$. Therefore, the false vacuum fraction evolves according to the equation

$$\frac{dF(t)}{dt} = F(t) \left[- \int_{t_i}^t dt' \Gamma(t') a(t')^3 \frac{d\bar{V}_b(t; t')}{dt} \right], \quad (2)$$

which can be directly solved as [84, 85]

$$F(t; t_i) = \exp \left[- \int_{t_i}^t dt' \Gamma(t') a(t')^3 \bar{V}_b(t; t') \right]. \quad (3)$$

Here t_i is the earliest moment when the bounce equation of ϕ ever allows for an instanton solution, and hence all regions are in the false vacuum before t_i , that is $F(t < t_i; t_i) = 1$. Due to the friction term in the bounce equation, t_i is slightly later than the critical time t_c when V_+ and V_- are degenerated. The comoving radius $r(t; t')$ in computing the comoving volume $\bar{V}_b(t; t') = \frac{4}{3} \pi r(t; t')^3$ of a true-vacuum bubble at t nucleated at an earlier time

t' can be estimated as

$$r(t; t') \equiv \frac{r_0}{a(t')} + \int_{t'}^t \frac{v_w(\tilde{t}) d\tilde{t}}{a(\tilde{t})} \approx (v_w \equiv 1) \int_{t'}^t \frac{d\tilde{t}}{a(\tilde{t})}, \quad (4)$$

where the initial bubble radius r_0 is usually ignored compared to its following expansion, and the full-time evolution of the bubble wall velocity $v_w(t)$ [86] is also ignored by directly taking its terminal value v_w to be unity for simplicity (the other constant value is a direct generalization, see, for example, Ref. [56]). The above false vacuum fraction function also defines a special moment t_{per} when most of the bubbles start to percolate with $F(t_{\text{per}}) = 0.7$ [87], roughly coinciding with the time t_* when the associated GW background peaks in its energy spectrum with maximal strength [88]. For any FOPT, it usually holds $t_c < t_i < t_{\text{nuc}} < t_{\text{per}} < t_*$. We will identify $t_* = t_{\text{per}}$ hereafter.

Finally, we depict the general picture of a cosmological FOPT inside and outside the delayed-decayed regions. Before the initial time for bubble nucleations, the Universe is dominated by radiation energy density diluted as $\rho_r(t < t_i) \propto a(t)^{-4}$ with an expanding scale factor $a(t)$, while the false vacuum energy density stays as a sub-dominated constant, $\rho_v(t < t_i) \equiv V_+ < \rho_r(t_i)$. Ever since the first nucleation of a bubble after the time t_i , the Universe is still globally dominated by radiations, but locally the delayed-decayed false vacuum regions are gradually dominated by the vacuum energy densities, and hence the scale factor would not be homogeneous anymore with more bubbles nucleated and percolated after rapid expansion and violent collisions. In both false vacuum and true vacuum regions, the radiations are still redshifted as $\rho_r(t > t_i, \mathbf{x}_+ | \phi(t, \mathbf{x}_+) = \phi_+) \propto a(t, \mathbf{x}_+)^{-4}$ and $\rho_r(t > t_i, \mathbf{x}_- | \phi(t, \mathbf{x}_-) = \phi_-) \propto a(t, \mathbf{x}_-)^{-4}$, respectively, but with different scale factors, while the vacuum energy densities stay at different constants $\rho_v(t > t_i, \mathbf{x}_+) \equiv V_+ > V_- \equiv \rho_v(t > t_i, \mathbf{x}_-)$. It is this vacuum-energy density difference $\Delta V \equiv V_+ - V_-$ that accumulates over time in false vacuum regions compared to true-vacuum regions with respect to rapidly diluted radiation energy

densities. Hence, the evolution equations read

$$\frac{d}{dt}\rho_r(t, \mathbf{x}_\pm) + 4H(t, \mathbf{x}_\pm)\rho_r(t, \mathbf{x}_\pm) = -\frac{d}{dt}\rho_v(t, \mathbf{x}_\pm), \quad (5)$$

$$3M_{\text{Pl}}^2 H(t, \mathbf{x}_\pm)^2 = \rho_r(t, \mathbf{x}_\pm) + \rho_v(t, \mathbf{x}_\pm), \quad (6)$$

where the spatial dependence \mathbf{x}_\pm can be attributed to different nucleation time of the first bubble locally in that patch with respect to the earliest nucleation time t_i globally, that is, $\rho_r(t, \mathbf{x}_\pm) = \rho_r(t; t_i + \Delta t(\mathbf{x}_\pm)) \equiv \rho_r(t; t_n(\mathbf{x}_\pm))$, correspondingly solved from $\rho_v(t, \mathbf{x}_+) \equiv \rho_v(t; t_n(\mathbf{x}_+)) = F(t; t_n)V_+$ and $\rho_v(t, \mathbf{x}_-) \equiv \rho_v(t; t_n(\mathbf{x}_-)) = [1 - F(t; t_n)]V_- = 0$ after setting the zero of the potential at V_- . Note here that the energy densities of expanding bubble walls have already been included in the total radiations as seen from directly estimating the equation of state [21, 72],

$$w_{\text{wall}} = \frac{p_{\text{wall}}}{\rho_{\text{wall}}} = \frac{\int dz \left[\frac{1}{2} \left(\frac{d\phi}{dt} \right)^2 - \frac{1}{6a^2} \left(\frac{d\phi}{dz} \right)^2 \right]}{\int dz \left[\frac{1}{2} \left(\frac{d\phi}{dt} \right)^2 + \frac{1}{2a^2} \left(\frac{d\phi}{dz} \right)^2 \right]} \approx \frac{1}{3}, \quad (7)$$

where we have used the approximation $d\phi/dt \approx d\phi/dz/a$ for the bubble wall velocity close to the speed of light. Even when bubble walls collide, they are still red-shifted as the dissipated thermal radiations and associated GW radiations. This evolutionary scaling for bubble walls is also consistent with the recent estimations [66, 67].

III. FALSE VACUUM ISLANDS

Solving the combined equations (3), (5), and (6) is inefficient as they are coupled integro-differential equations of the scale factors in inhomogeneous regions. One rigorous method is to solve Eqs. (5) and (6) iteratively with some initial test form for the scale factor in the false vacuum fraction (3) as done recently in Ref. [68], which might still be inefficient for our later purpose to calculate the curvature perturbations. The other approach is to transform the two-dimensional system of integro-differential equations into a seven-dimensional system of first-order ordinary differential equations as proposed recently in Ref. [69], which we will pursue in future studies. In this study, we will adopt an approximated strategy. For a general FOPT that can be completed appropriately [84, 85, 89], the global evolutions before and after the FOPT are both dominated by radiations diluted as $\rho_r(t) \propto a(t)^{-4}$ with the scale factor $a(t) \propto t^{1/2}$. However, the radiation energy densities right before and after the FOPT will differ by the released vacuum energy densities that turn into radiation-like walls, and hence there is a step-like jumping in the time evolution of total radiations, during which the radiations are always red-shifted as $\rho_r \propto a^{-4}$ but the scale factor would expand faster

than $a(t) \propto t^{1/2}$. The approximated strategy we adopt is to effectively transfer the inhomogeneities in the scale factors into the equation of state of inhomogeneous distributions of radiations. This is done by first fixing the scale factor in the false vacuum fraction (3) as in the radiation-dominated era with $a(t) \propto t^{1/2}$ throughout the FOPT as shown in the left panel of Fig. 2,

$$F(\bar{t}; \bar{t}_n) = \exp \left[-\frac{4}{3} \pi \Theta(\bar{t} - \bar{t}_n) \int_{\bar{t}_n}^{\bar{t}} dt' e^{\beta \bar{t}'} 8 \left(\sqrt{t'} - t' \right)^3 \right], \quad (8)$$

and then solve the dimensionless version of the dynamical equations (5) and (6),

$$\frac{d}{d\bar{t}} \bar{\rho}_r(\bar{t}; \bar{t}_n) + 4\sqrt{\bar{\rho}_r(\bar{t}; \bar{t}_n) + \bar{\alpha} F(\bar{t}; \bar{t}_n)} \bar{\rho}_r(\bar{t}; \bar{t}_n) = -\bar{\alpha} \dot{F}(\bar{t}; \bar{t}_n), \quad (9)$$

with an initial condition deep into the radiation era,

$$\bar{\rho}_r(\bar{t}_{\text{ini}}; \bar{t}_n) = \frac{1}{4\bar{t}_{\text{ini}}^2} - \bar{\alpha}, \quad (10)$$

where the dimensionless radiation density $\bar{\rho}_r(\bar{t}; \bar{t}_n) \equiv \rho_r(\bar{t}; \bar{t}_n)/(3M_{\text{Pl}}^2 \Gamma_0^{1/2})$ is defined with respect to a characteristic density scale $\rho_\Gamma \equiv 3M_{\text{Pl}}^2 \Gamma_0^{1/2} \equiv 3M_{\text{Pl}}^2 H_\Gamma^2$ that can be used to normalize a dimensionless strength factor $\bar{\alpha} \equiv \Delta V/\rho_\Gamma$. Thus, the initial condition is obtained by

$$\begin{aligned} \bar{\rho}_r(\bar{t}_{\text{ini}}; \bar{t}_n) &\equiv \frac{\rho_r(\bar{t}_{\text{ini}}; \bar{t}_n)}{3M_{\text{Pl}}^2 H_\Gamma^2} = \frac{3M_{\text{Pl}}^2 H_{\text{ini}}^2}{3M_{\text{Pl}}^2 H_\Gamma^2} - \frac{\rho_v(\bar{t}_{\text{ini}}; \bar{t}_n)}{\rho_\Gamma} \\ &= \left(\frac{H_{\text{ini}} t_{\text{ini}}}{\Gamma_0^{1/4} t_{\text{ini}}} \right)^2 - \frac{F(\bar{t}_{\text{ini}}; \bar{t}_n) \Delta V}{\rho_\Gamma} = \frac{1}{4\bar{t}_{\text{ini}}^2} - \bar{\alpha}, \end{aligned} \quad (11)$$

where we have used $H_{\text{ini}} t_{\text{ini}} = 1/2$ for any initial time $t_{\text{ini}} \ll t_i$ sufficiently deep into the radiation dominance without nucleating any bubble yet with $F(\bar{t}_{\text{ini}}; \bar{t}_n) = 1$.

Therefore, the normal decayed regions can be solved from (8), (9), and (10) by fixing the nucleation time of the first bubble at the earliest nucleation time globally, that is $t_n = t_i$, while the delayed-decayed regions can be solved from (8), (9), and (10) by choosing any nucleation time $t_n > t_i$ later than the global one. The global initial nucleation time \bar{t}_i can be arbitrarily fixed as long as it meets $\bar{t}_i < \bar{t}_{\text{nuc}} \equiv \Gamma_0^{1/4} t_{\text{nuc}} = H_{\text{nuc}} t_{\text{nuc}} e^{-\beta/(8H_{\text{nuc}})} \approx (1/2)e^{-W(\bar{\beta}/8)} = (4/\bar{\beta})W(\bar{\beta}/8)$ from recalling that $\Gamma_0^{1/4} \equiv H_{\text{nuc}} e^{-\beta/(8H_{\text{nuc}})}$, $H_{\text{nuc}} t_{\text{nuc}} \approx 1/2$, and $\beta/(8H_{\text{nuc}}) \approx W(\bar{\beta}/8)$. It is worth noting that, both the model parameters $\bar{\alpha} \equiv \Delta V/(3M_{\text{Pl}}^2 \Gamma_0^{1/2})$ and $\bar{\beta} \equiv \beta/\Gamma_0^{1/4}$ are not equal to the physical strength and duration parameters α_* and $(\beta/H)_*$ defined phenomeno-

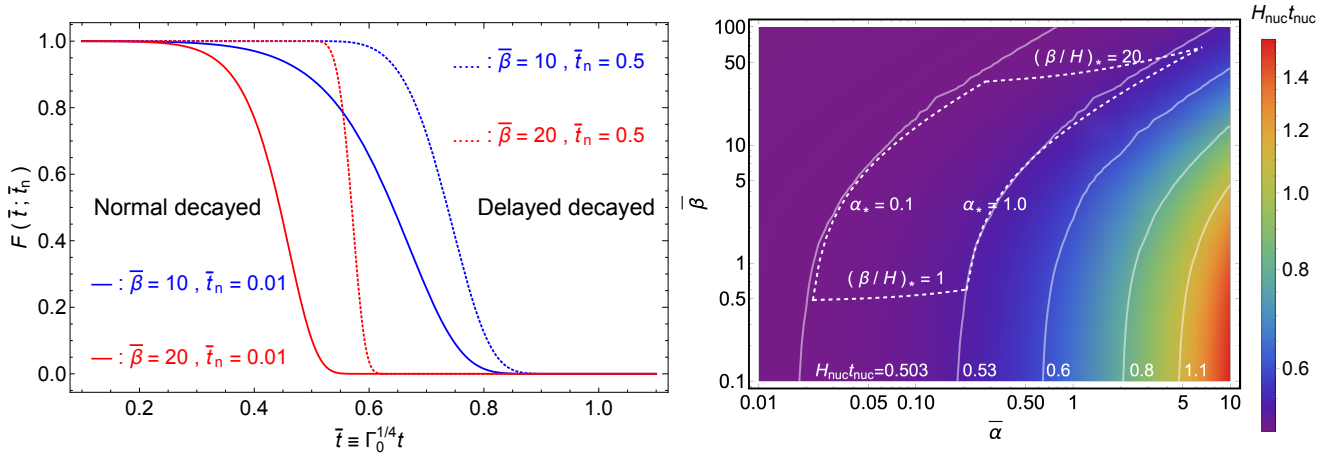


FIG. 2. *Left*: The time evolution of the false vacuum fraction given earlier (solid) and later (dashed) nucleation times of the first bubble with shorter (red) and longer (blue) duration times. *Right*: The physical (phenomenological) strength and duration parameters are bounded in the region with $0.1 < \alpha_* < 1.0$ and $1 < (\beta/H)_* < 20$ (dashed) given the model parameters $\bar{\alpha}$ and $\bar{\beta}$. The approximation $H_{\text{nuc}} t_{\text{nuc}} \approx 1/2$ is checked with solid contour curves.

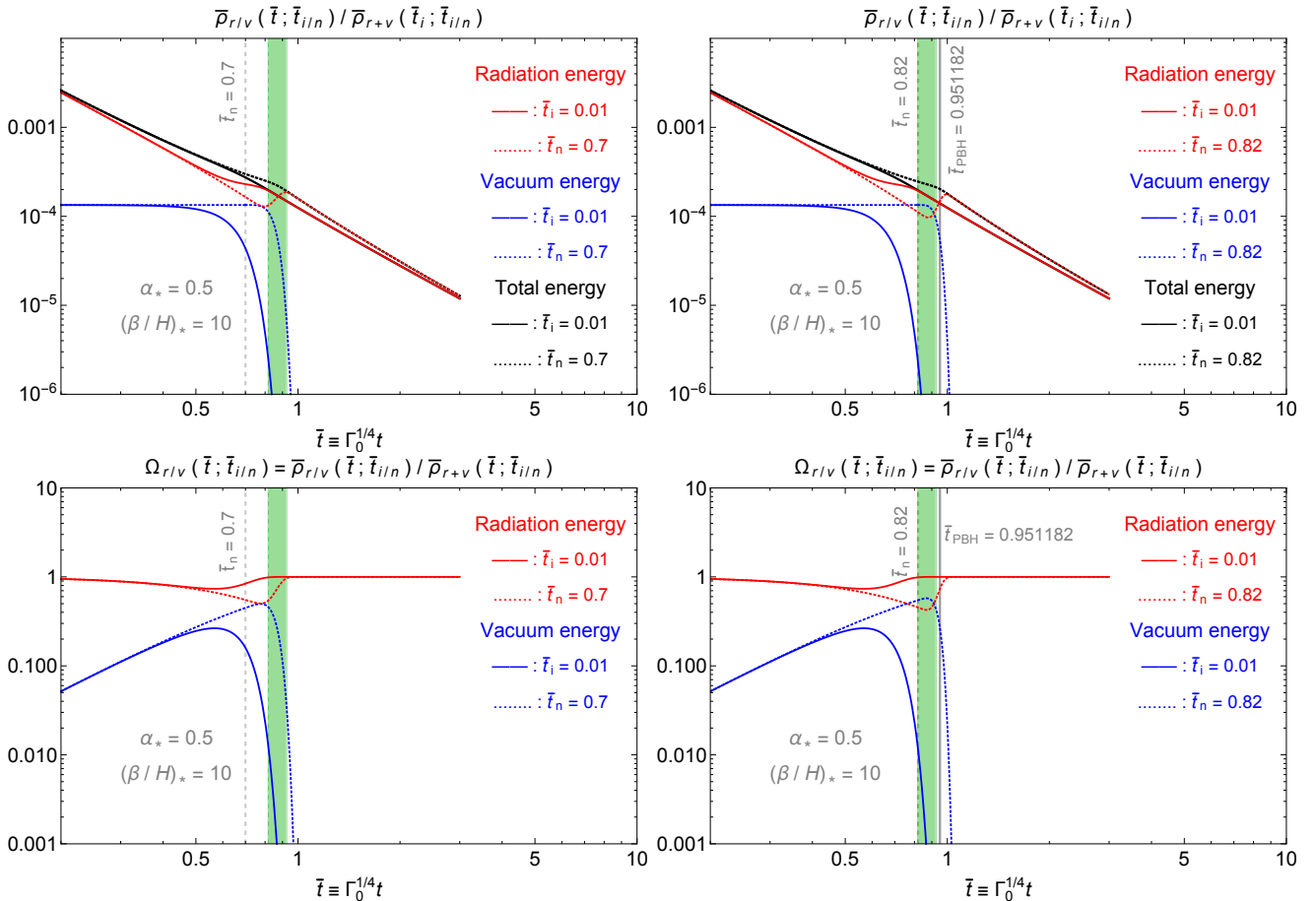


FIG. 3. The time evolutions of energy densities with respect to the total density at the initial nucleation time (top) and the real time (bottom) for radiations (red) and vacuum (blue) components as well as their combined (black) in the normal-decayed (solid) and delayed-decayed (dashed) regions during an illustrative FOPT with a strength parameter $\alpha_* = 0.5$ and a duration parameter $(\beta/H)_* = 10$. PBHs can be formed at the latest at the gray vertical line (right) for a delayed-decayed nucleation time at the earliest at the left boundary of the green band, below which no PBH can be produced (left).

logically for general cosmological FOPTs by

$$\alpha_* = \frac{\Delta V}{\rho_r(t_{\text{per}}; \bar{t}_i)} = \frac{\bar{\alpha}}{\bar{\rho}_r(\bar{t}_{\text{per}}; \bar{t}_i)}, \quad (12)$$

$$\left(\frac{\beta}{H}\right)_* = \frac{\beta/\Gamma_0^{1/4}}{\sqrt{H_*^2/\Gamma_0^{1/2}}} = \frac{\bar{\beta}}{\sqrt{\bar{\rho}_{\text{tot}}(\bar{t}_{\text{per}}; \bar{t}_i)}}, \quad (13)$$

where the total dimensionless density is generally defined as $\bar{\rho}_{\text{tot}}(\bar{t}; \bar{t}_n) \equiv \bar{\rho}_r(\bar{t}; \bar{t}_n) + \bar{\rho}_v(\bar{t}; \bar{t}_n) = \bar{\rho}_r(\bar{t}; \bar{t}_n) + \bar{\alpha}F(\bar{t}; \bar{t}_n)$. In this paper, we will illustrate with a general FOPT in the physical parameter space bounded by $0.1 < \alpha_* < 1.0$ and $1 < (\beta/H)_* < 20$, which can be mapped onto the model parameter space in the $\bar{\alpha} - \bar{\beta}$ plane as shown in the right panel of Fig. 2 with the approximated relation $H_{\text{nuc}} t_{\text{nuc}} \approx 1/2$ checked by the colored contoured regions. In this parameter region, we can safely choose the global initial nucleation time at $\bar{t}_i = 0.01$, any other values comparable or earlier than this one are also allowable.

IV. PRIMORDIAL BLACK HOLES

Given the model parameters $\bar{\alpha}$ and $\bar{\beta}$, both the radiation energy density $\bar{\rho}_r(\bar{t}; \bar{t}_n)$ and (false) vacuum energy density $\bar{\rho}_v(\bar{t}; \bar{t}_n) \equiv \bar{\alpha}F(\bar{t}; \bar{t}_n)$ can be directly solved in the normal-decayed and delayed-decayed regions with $\bar{t}_n = \bar{t}_i$ and $\bar{t}_n > \bar{t}_i$, respectively. Note that one can use these solutions to directly compute the physical strength and duration parameters via (12), which can also be used inversely to determine the model parameters $\bar{\alpha}$ and $\bar{\beta}$ in terms of the physical parameters α_* and $(\beta/H)_*$. The time evolutions of these solutions are presented in Fig. 3 for an illustrative FOPT with physical strength factor $\alpha_* = 0.5$ and inverse duration $(\beta/H)_* = 10$ with (right) and without (left) the outcome of PBH formations. To see when PBHs can form, we first define the energy density contrast in the delayed-decayed regions with respect to the normal-decayed regions as

$$\delta(\bar{t}; \bar{t}_n, \bar{t}_i) = \frac{\bar{\rho}_r(\bar{t}; \bar{t}_n) + \bar{\rho}_v(\bar{t}; \bar{t}_n)}{\bar{\rho}_r(\bar{t}; \bar{t}_i) + \bar{\rho}_v(\bar{t}; \bar{t}_i)} - 1, \quad (14)$$

where we choose the normal-decayed regions in the denominator with the earliest possible nucleation time of the first bubble globally. This is justified as the probability of staying in the false vacuum to accumulate (false) vacuum energy density is exponentially suppressed by another exponential approximately. That is to say, a region with some local nucleation time is more probably surrounded by the regions with earlier nucleation times, and hence the local energy density contrast always tends to be over-dense rather than under-dense, which can be effectively achieved by choosing the nucleation time in the denominator as the global one.

Next, we turn to the overdensity evolution as shown in Fig. 4, where the right panel is just a zoom-in view of the left panel, and all vertical dashed lines are the

corresponding local nucleation times with possible PBH formation times as shown with vertical solid lines. For a longer enough delayed decay time \bar{t}_n as shown with the purple curve in the right panel, it is always possible to locate a time \bar{t}_{PBH} for surpassing the PBH threshold with $\delta(\bar{t}_{\text{PBH}}; \bar{t}_n, \bar{t}_i) = \delta_c$ at the vertical purple line in the right panel. However, there is a lower bound on the delayed decay time \bar{t}_n^{min} as shown with a vertical blue dashed line, below which the overdensity never reaches the PBH threshold $\delta_c = 0.45$ [90, 91] as shown with the red curve. That is to say, for a delayed-decayed region with this local nucleation time \bar{t}_n^{min} as shown with the blue curve, the overdensity would saturate the PBH threshold exactly at the maximum of the overdensity evolution,

$$\delta(\bar{t}_{\text{PBH}}^{\text{max}}; \bar{t}_n^{\text{min}}, \bar{t}_i) = \delta_c, \quad (15)$$

$$\left. \frac{d}{d\bar{t}} \delta(\bar{t}; \bar{t}_n^{\text{min}}, \bar{t}_i) \right|_{\bar{t}=\bar{t}_{\text{PBH}}^{\text{max}}} = 0, \quad (16)$$

$$\left. \frac{d^2}{d\bar{t}^2} \delta(\bar{t}; \bar{t}_n^{\text{min}}, \bar{t}_i) \right|_{\bar{t}=\bar{t}_{\text{PBH}}^{\text{max}}} < 0. \quad (17)$$

Here the maximum point is denoted by $\bar{t}_{\text{PBH}}^{\text{max}}$ as this is the latest time for PBH formations as shown with the vertical blue solid line. To see this, note that regions with earlier nucleation time (for example, the blue curve) will accumulate the overdensity slower than regions with later nucleation time (for example, the purple curve), and hence will form PBHs at a later time as shown with the vertical blue solid line compared to the vertical purple solid line. Therefore, the earliest possible nucleation time \bar{t}_n^{min} would correspond to the latest possible PBH formation time $\bar{t}_{\text{PBH}}^{\text{max}}$. Similarly, there is also an upper bound on the delayed decay nucleation time \bar{t}_n^{max} as shown with the vertical green dashed line, in which case the local nucleation time \bar{t}_n is late enough so that the corresponding PBH formation time \bar{t}_{PBH} becomes early enough to exactly coincide with the local nucleation time so that the PBH threshold $\delta(\bar{t}_{\text{PBH}}^{\text{min}}; \bar{t}_n^{\text{max}}, \bar{t}_i) = \delta_c$ is exactly found when $\bar{t}_n^{\text{max}} = \bar{t}_{\text{PBH}}^{\text{min}}$ as shown with the vertical green dashed/solid lines. Except for this critical case, all delayed-decayed regions have already started the process of bubble nucleation before PBH formations as stressed recently in Ref. [66].

Finally, we determine that the most probable time for PBH formations is $\bar{t}_{\text{PBH}}^{\text{max}}$ since it corresponds to the earliest delayed decay nucleation time \bar{t}_n^{min} , after which the probability of staying at the false vacuum for such a long time is exponentially suppressed by another exponential, and hence the corresponding PBH abundance must be negligible. Therefore, the PBH mass function $f_{\text{PBH}}(M_{\text{PBH}})$ for our accumulating mechanism is almost monochromatic. For the sake of most generality, we will estimate the PBH mass function for arbitrary $t_n^{\text{min}} \leq \bar{t}_n \leq \bar{t}_n^{\text{max}}$ and corresponding $\bar{t}_{\text{PBH}}^{\text{min}} \leq \bar{t}_{\text{PBH}} \leq \bar{t}_{\text{PBH}}^{\text{max}}$. The PBH mass $M_{\text{PBH}} = \gamma \left(\frac{4}{3}\pi H_{\text{PBH}}^{-3}\right) (3M_{\text{pl}}^2 H_{\text{PBH}}^2)$ collapsed

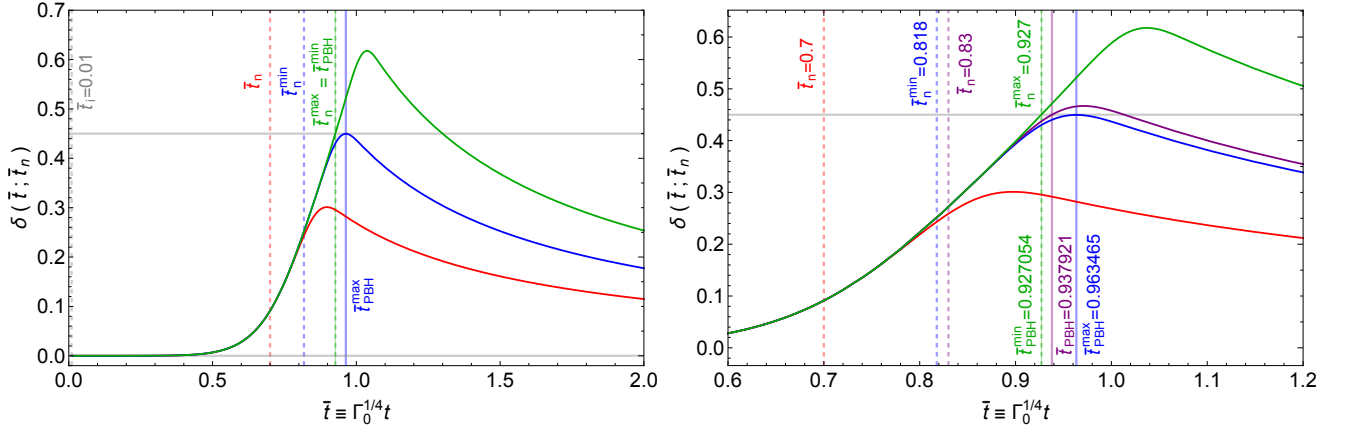


FIG. 4. The time evolution of the overdensity (left) and its zoom-in view (right) in the delayed-decayed region during a FOPT with illustrative strength factor $\alpha_* = 0.5$ and inverse duration $(\beta/H)_* = 10$, where vertical dashed lines are different delayed-decayed nucleation times of the first bubble with possible PBH formation at later times as shown with vertical solid lines.

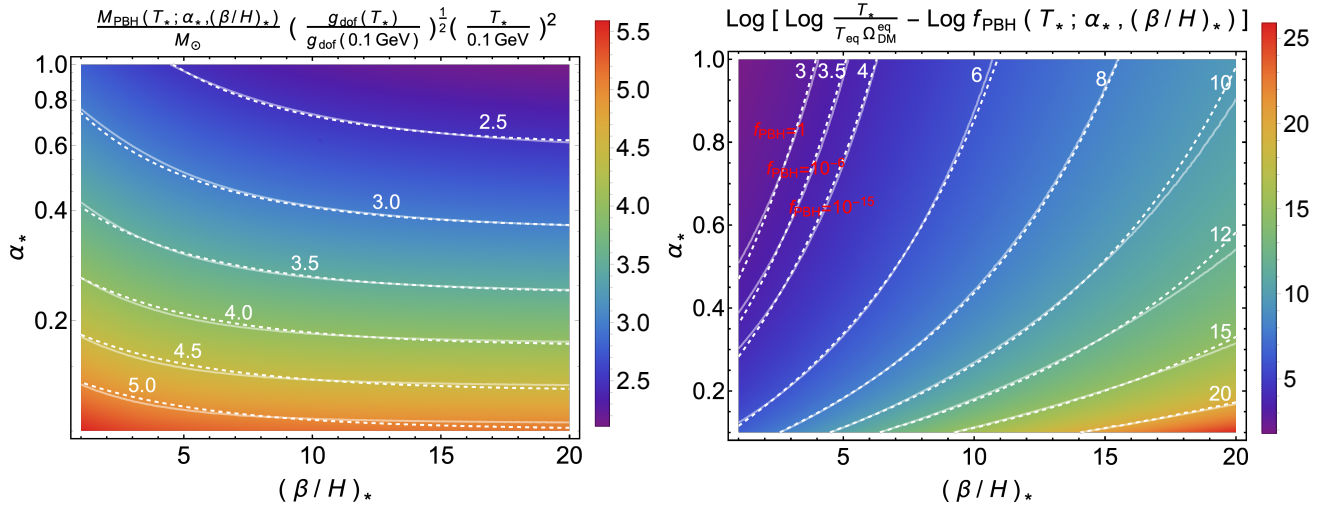


FIG. 5. The fitting formulas (dashed) to the PBH mass (left) and abundance (right) given the FOPT parameters from the strength factor α_* , inverse duration $(\beta/H)_*$, and percolation temperature T_* for the most probable case of PBH formations.

from the Hubble-scale horizon mass at \bar{t}_{PBH} reads

$$\frac{M_{\text{PBH}}}{M_{\odot}} = 4\pi\gamma \frac{M_{\text{Pl}}}{M_{\odot}} \frac{M_{\text{Pl}}/\Gamma_0^{1/4}}{H_{\text{PBH}}/\Gamma_0^{1/4}}, \quad (18)$$

where $\gamma_{\text{PBH}} = 0.2$ [92], $M_{\text{Pl}}/M_{\odot} = 2.182 \times 10^{-39}$, and $\bar{H}_{\text{PBH}} \equiv H_{\text{PBH}}/\Gamma_0^{1/4} = \sqrt{\bar{\rho}_{\text{tot}}(\bar{t}_{\text{PBH}}; \bar{t}_n)}$, while the remaining factor can be approximately estimated as

$$\frac{\Gamma_0^{1/4}}{M_{\text{Pl}}} = \left(\frac{\pi^2}{90} g_{\text{dof}}\right)^{1/2} \left(\frac{T_*}{M_{\text{Pl}}}\right)^2 \frac{\bar{t}_*}{\bar{t}_{\text{nuc}}} e^{-W(\frac{\bar{\beta}}{8})} \quad (19)$$

by recalling $\Gamma_0^{1/4} \equiv H_{\text{nuc}} e^{-\beta/(8H_{\text{nuc}})}$ with $3M_{\text{Pl}}^2 H_{\text{nuc}}^2 \approx (\pi^2/30) g_{\text{dof}} T_{\text{nuc}}^4$, $(T_{\text{nuc}}/T_*)^2 = \bar{t}_*/\bar{t}_{\text{nuc}}$, and $\beta/(8H_{\text{nuc}}) \approx W(\bar{\beta}/8)$. Here \bar{t}_* is solved from $F(\bar{t}_*; \bar{t}_n) = 0.7$ and $\bar{t}_{\text{nuc}} \approx (4/\bar{\beta})W(\bar{\beta}/8)$ is determined from $\bar{\beta}$ that can be further

determined from given α_* and $(\beta/H)_*$. Note here that T_* is another input parameter in addition to the strength factor α_* and inverse duration $(\beta/H)_*$ for estimating the PBH mass function. For the most probable case of PBH formations with $\bar{t}_n = \bar{t}_n^{\text{min}}$ and $\bar{t}_{\text{PBH}} = \bar{t}_{\text{PBH}}^{\text{max}}$, we have found a ready-to-use fitting formula for the PBH mass,

$$M_{\text{PBH}} = 3M_{\odot} \left(\frac{g_{\text{dof}}(0.1 \text{ GeV})}{g_{\text{dof}}(T_*)}\right)^{1/2} \left(\frac{T_*}{0.1 \text{ GeV}}\right)^{-2} \times \text{Fit}_M \left(\frac{\alpha_*}{0.6}, \frac{(\beta/H)_*}{3} - 1\right), \quad (20)$$

where the last factor in the fitting formula admits a simple form from combinations of power-law and exponential

terms as

$$\text{Fit}_M(A, B) = \frac{1}{3} + \frac{1}{6}e^{-\frac{B}{2}} + \frac{A^{-0.55}}{2} - \frac{A^{-0.55}}{100}e^{-\frac{B}{2}}. \quad (21)$$

The PBH abundance $f_{\text{PBH}} = (a_{\text{eq}}/a_{\text{PBH}})\Omega_{\text{PBH}}/\Omega_{\text{DM}}^{\text{eq}}$ normalized to the dark matter fraction $\Omega_{\text{DM}}^{\text{eq}} = 0.42$ at the matter-radiation equality can be estimated from noting that the PBH fraction $\Omega_{\text{PBH}}(\bar{t}_{\text{PBH}})$ at formation time is exactly the probability $P(t_n)$ for a Hubble volume $V_H(t) = \frac{4}{3}\pi H(t)^{-3}$ not to decay until the delayed-decayed nucleation time \bar{t}_n . This can be further broken into infinite time intervals, $P(t_n) = \prod_{t=\bar{t}_i}^{\bar{t}_n} dP(t)$, each of which can be approximated as $dP(t) = 1 - \Gamma(t)V_H(t)dt \approx \exp[-\Gamma(t)V_H(t)dt]$ for this Hubble volume not to decay within the time interval dt at the time t . Therefore, the PBH fraction at formation time reads

$$\begin{aligned} \Omega_{\text{PBH}}(\bar{t}_{\text{PBH}}) &= P(\bar{t}_n) = \exp\left[-\int_{\bar{t}_i}^{\bar{t}_n} dt\Gamma(t)V_H(t)\right] \\ &= \exp\left[-\frac{4}{3}\pi\int_{\bar{t}_i}^{\bar{t}_n} d\bar{t}e^{\beta\bar{t}}\left(\frac{\sqrt{\bar{t}/\bar{t}_{\text{PBH}}}}{\bar{H}_{\text{PBH}}}\right)^3\right]. \end{aligned} \quad (22)$$

The remaining factor $a_{\text{eq}}/a_{\text{PBH}} = T_{\text{PBH}}/T_{\text{eq}}$ with $T_{\text{eq}} \approx 0.75$ eV can be estimated by approximating $3M_{\text{Pl}}^2 H_{\text{PBH}}^2 = (\pi^2/30)g_{\text{dof}}T_{\text{PBH}}^4$ after replacing $H_{\text{PBH}} = \bar{H}_{\text{PBH}}\Gamma_0^{1/4}$ with previously computed \bar{H}_{PBH} and $\Gamma_0^{1/4}/M_{\text{Pl}}$, that is,

$$\frac{T_{\text{PBH}}}{M_{\text{Pl}}} = \bar{\rho}_{\text{tot}}^{1/4}(\bar{t}_{\text{PBH}}; \bar{t}_n) \left(\frac{T_*}{M_{\text{Pl}}}\right) \left(\frac{\bar{t}_*}{\bar{t}_{\text{nuc}}}\right)^{\frac{1}{2}} e^{-\frac{1}{2}W\left(\frac{\beta}{3}\right)}. \quad (23)$$

It is worth noting that the PBH abundance admits no dependence on the relativistic effective degrees of freedom g_{dof} as it is canceled out in evaluating $T_{\text{PBH}}/M_{\text{Pl}}$. For the most probable case of PBH formations with $\bar{t}_n = \bar{t}_n^{\text{min}}$ and $\bar{t}_{\text{PBH}} = \bar{t}_{\text{PBH}}^{\text{max}}$, we have found a ready-to-use fitting formula for the PBH abundance,

$$f_{\text{PBH}} = \frac{T_*}{T_{\text{eq}}\Omega_{\text{DM}}^{\text{eq}}} \exp\left\{-\exp\left[\text{Fit}_f\left(\frac{\alpha_*}{0.6}, \frac{(\beta/H)_*}{3} - 1\right)\right]\right\}, \quad (24)$$

where the last factor in the fitting formula admits a simple form from combinations of power-law and linear terms as $\text{Fit}_f(A, B) = 3[(U + XA^{-m}) + (V + YA^{-n})B]$ with $U = -0.93$, $V = 0.32$, $X = 2.11$, $Y = 0.17$, $m = 0.32$, and $n = 0.81$. The goodness of fit for the PBH mass and abundance can be seen in Fig. 5 with the fitting formulas shown in white dashed contours.

A typical benchmark point reads $M_{\text{PBH}} = 3M_{\odot}$ and $f_{\text{PBH}} = 6 \times 10^{-7}$ for $\alpha_* = 0.6$, $(\beta/H)_* = 3$, and $T_* = 0.1$ GeV, providing a promising PBH origin for the recent mass-gap observations from PSR J0514-4002E [102, 103] and GW230529 181500 [104] events, the later of which can meet the newly estimated abundance $f_{\text{PBH}} \sim 10^{-3}$ [105] if we adopt $\alpha_* = 0.7$, $(\beta/H)_* = 3$, and

$T_* = 0.1$ GeV. Since the PBH mass is almost sensitive to the FOPT scale alone, other typical PBH masses can be exemplified with different percolation temperatures T_* as shown in Fig. 6, where associated PBH abundances can touch the boundaries of current PBH constraints [93] (with GW constraints replaced by recent updates [94–96]) by tuning the strength factors α_* with respect to the inverse durations $(\beta/H)_* = 4$ (vertical dashed lines) and $(\beta/H)_* = 3$ (vertical solid lines) as the PBH abundance is more sensitive to $(\beta/H)_*$ than α_* . Therefore, all PBH mass ranges including the asteroid-mass PBH as all dark matter, the planet-mass PBH as weak lensing events, solar-mass PBH as LIGO-Virgo events, and supermassive black holes as in the galactic center can be easily realized with FOPTs at PeV, TeV, MeV, and keV scales.

V. CURVATURE PERTURBATIONS

The highly inhomogeneous evolution among radiations and vacuum energy densities would certainly induce curvature perturbations from the accumulated overdensity perturbations in different regions with different local nucleation times \bar{t}_n of the first bubbles compared to the background with the earliest possible global nucleation time \bar{t}_i . In this section, we will estimate the curvature perturbations in real space by summing over all possible nucleation histories. For later convenience, we introduce a dimensionless version $\bar{V}_R(t) \equiv \Gamma_0^{3/4}V_R(t)$ of the physical volume at a time t for a delayed-decayed region $V_R(t) = \frac{4}{3}\pi(a(t)R)^3$ of a comoving size R ,

$$\frac{4}{3}\pi\left[\sqrt{\Gamma_0^{1/4}t}\left(C_0\Gamma_0^{1/8}R\right)\right]^3 \equiv \frac{4}{3}\pi\left(\sqrt{\bar{t}}\bar{R}\right)^3 \equiv \bar{V}_R(\bar{t}), \quad (25)$$

where the scale factor is dominated by radiation as $a(t) = C_0t^{1/2}$ recalling our effective approximation by transferring the inhomogeneities in scale factors temporarily into the equation of state, while the introduced dimensionless comoving scale $\bar{R} \equiv (C_0\Gamma_0^{1/8}R)$ serves as a convenient notation when the scale enters the Hubble horizon at t_R by $\bar{R}_H^{-1} = a(t_R)H(t_R)/(C_0\Gamma_0^{1/8}) = \sqrt{\bar{t}_R}\bar{H}(\bar{t}_R) = \sqrt{\bar{t}_R}\bar{\rho}_{\text{tot}}(\bar{t}_R; \bar{t}_i)$. Then, we calculate the probability for this region $\bar{V}_R(\bar{t})$ not to decay until a time t' , that is,

$$\begin{aligned} P_R(t') &= \exp\left[-\int_{\bar{t}_i}^{\bar{t}'} d\bar{t}e^{\beta\bar{t}}\bar{V}_R(\bar{t})\right] \\ &= \exp\left[\frac{4}{3}\pi\bar{R}^3\bar{t}^{\frac{5}{2}}E_{-\frac{3}{2}}(-\beta\bar{t})\Big|_{\bar{t}_i}^{\bar{t}'}\right] \equiv \bar{P}_R(\bar{t}'), \end{aligned} \quad (26)$$

where $E_n(z) \equiv \int_1^\infty e^{-zt}t^{-n}dt$ is the exponential integral.

Next, we define the smoothed density contrast field at a comoving scale R by $\delta_R(t, \mathbf{x}) = \int d^3\mathbf{x}'W_R(|\mathbf{x} - \mathbf{x}'|)\delta(t, \mathbf{x})$

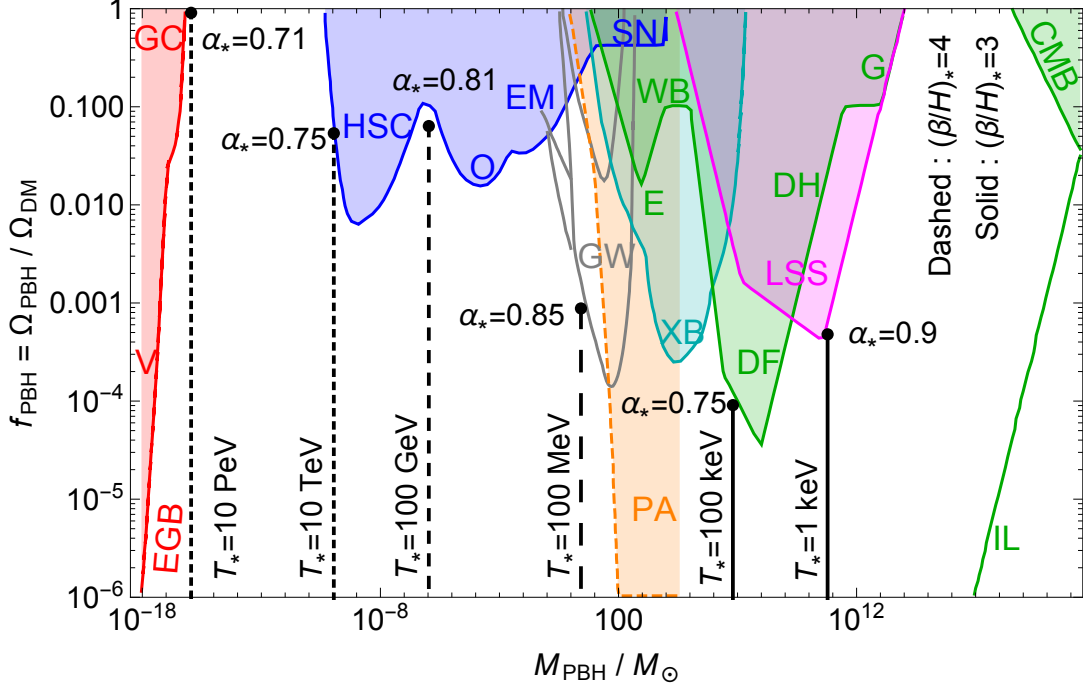


FIG. 6. Illustrative examples of FOPTs at different percolation temperatures T_* with different strength factors α_* and inverse durations $(\beta/H)_* = 4$ (vertical dashed lines) and $(\beta/H)_* = 3$ (vertical solid lines), in which cases the associate PBH masses and abundances roughly reach the boundaries of current PBH constraints from the collection [93] (and references therein but with GW constraints replaced by recent updates [94–96]). Note that the micro-lensing constraints from Subaru/HSC Andromeda observations [97] and Optical Gravitational Lensing Experiment (OGLE) [98] (recently updated in Refs. [99, 100] for OGLE III+OGLE IV) could be significantly enhanced for PBHs dressed with dark matter minihalos [101].

with some window function $W_R(r) = 3\Theta(R-r)/(4\pi R^3)$. To calculate the variance of density perturbations at a comoving smoothing scale R , $\sigma_\delta^2(t; R) \equiv \langle (\delta_R(t, \mathbf{x}) - \langle \delta_R(t, \mathbf{x}) \rangle)^2 \rangle = \langle \delta_R^2(t, \mathbf{x}) \rangle - \langle \delta_R(t, \mathbf{x}) \rangle^2$, recall that the spatial dependence in the density $\rho(t, \mathbf{x}) = \rho(t; t_i + \Delta t(\mathbf{x})) \equiv \rho(t; t_n)$ comes from different local nucleation times of the first bubble in that region compared to the background with the earliest possible global nucleation time t_i , and hence the average value for the overdensity $\delta(t, \mathbf{x}) \equiv \rho(t; t_n)/\rho(t; t_i) - 1 \equiv \delta(t; t_n)$ at some comoving smoothing scale R can be calculated by summing over all regions of size R that had not yet decayed until the time considered,

$$\begin{aligned} \langle \delta_R(t, \mathbf{x}) \rangle_{\mathbf{x}} &\equiv \langle \delta_R(t; t_i + \Delta t(\mathbf{x})) \rangle_{\mathbf{x} \in \mathbb{R}^3/R^3} \equiv \langle \delta(t; t_n) \rangle_{t_n} \\ &= \int_{t_i}^{U(t)} \delta(t; t') P_R(t') \Gamma(t') V_R(t') dt', \end{aligned} \quad (28)$$

where \mathbb{R}^3/R^3 is a quotient set differed by a scale R , while the upper bound for the nucleation time integration reads

$$U(t) = \begin{cases} t_n^{\max}, & t < t_n^{\max} \equiv t_{\text{PBH}}^{\min}, \\ t_n(t), & t_n^{\max} \equiv t_{\text{PBH}}^{\min} < t < t_{\text{PBH}}^{\max}, \\ t_n^{\min}, & t > t_{\text{PBH}}^{\max}. \end{cases} \quad (29)$$

The choice for the upper-bound function $U(t)$ is the key part of our proposal for the nucleation history sum-

mation, which merits further elaborations as below: (i) For the time considered smaller than the earliest possible time for PBH formations, $t < t_n^{\max} \equiv t_{\text{PBH}}^{\min}$, all regions of size R will contribute to the above integration, and hence the upper bound $U(t) = t_n^{\max}$ should cover all the possible delayed-decayed nucleation times regardless whether or not these regions can eventually collapse into PBHs. (ii) For the time considered within the possible time interval for PBH formations, $t_{\text{PBH}}^{\min} < t < t_{\text{PBH}}^{\max}$, all regions of size R except for those regions that have already collapsed into PBHs should contribute to the above integration. Since regions that decay later would collapse into PBHs earlier, and hence we can solve the condition $\delta(t; t_n(t), t_i) = \delta_c$ for the upper bound $U(t) = t_n(t)$, beyond which those regions have already collapsed into PBHs by the time t . (iii) For the time considered larger than the latest possible time for PBH formation, all regions that can collapse into PBHs should be left out of the above integration, and hence the upper bound $U(t) = t_n^{\min}$ should only cover those regions with the local nucleation times not late enough to produce PBHs. The above procedure of nucleation history summation can also be used to calculate the average value for any function of the filtered density field as

$$\langle f(\delta_R(\bar{t})) \rangle = \int_{t_i}^{U(\bar{t})} f(\delta(\bar{t}; \bar{t}')) \bar{P}_R(\bar{t}') e^{\bar{\beta} \bar{t}'} \bar{V}_R(\bar{t}') d\bar{t}'. \quad (30)$$

Then, we can directly compute the variance of the accumulated overdensity field smoothed at a comoving scale R by $\sigma_\delta^2(\bar{t}; \bar{R}) = \langle \delta_{\bar{R}}(\bar{t})^2 \rangle - \langle \delta_{\bar{R}}(\bar{t}) \rangle^2$, which can be particularly evaluated at a specific comoving scale $\bar{R}_H^{-1} = a(t_R)H(t_R)$ that enters the Hubble horizon roughly around the percolation time t_* , that is $t_{RH} = t_*$. The resulting standard deviation of the overdensity perturbation $\sigma_\delta(\bar{t}_*; \bar{R}_{H_*} = 1/\sqrt{\bar{t}_* \bar{\rho}_{\text{tot}}(\bar{t}_*; \bar{t}_i)})$ around bubble percolation time can be shown in the top row of Fig. 7, whose parameter dependence on the strength factor α_* is almost linear and the parameter dependence on the inverse duration $(\beta/H)_*$ should asymptotic to power of $-5/2$ at the large inverse duration limit as argued in Refs [72, 75]. This combined leads to the heuristic scaling $\sigma_\delta(\bar{t}_*; \bar{R}_{H_*}) \sim \alpha_* (\beta/H)_*^{-5/2}$.

Finally, we can turn to calculate the power spectrum for the overdensity perturbations and the associated curvature perturbations. The basic strategy is to transform the definite integral of $\sigma_\delta^2(t; R)$ into a definite integral with a variable upper limit by a k -space top-hat window function,

$$\sigma_\delta^2(t; R) = \int_0^\infty \frac{dk}{k} \widetilde{W}_R^2(k) \mathcal{P}_\delta(t, k) \approx \int_0^{k_\Lambda} \frac{dk}{k} \mathcal{P}_\delta(t, k), \quad (31)$$

where the choice for the cut-off scale k_Λ is not unique. A natural but naive choice would be $k_\Lambda = 1/R$ [106, 107]. Another plausible choice $k_\Lambda = 3\pi/(5R)$ can be obtained from requiring the same normalization $k_\Lambda \equiv \int_0^{k_\Lambda} dk = \int_0^\infty dk \widetilde{W}_R^2(k) = 3\pi/(5R)$ for the Fourier transformed window function $\widetilde{W}_R(k) = 3j_1(kR)/(kR)$. The previous choice [72] for the window function with a Gaussian form $\widetilde{W}_R(k) = \exp(-k^2 R^2/2)$ renders a much smaller cutoff $k_\Lambda \equiv \int_0^{k_\Lambda} dk = \int_0^\infty dk \widetilde{W}_R^2(k) = \sqrt{\pi}/(2R)$. We further test and present in this paper a relatively compromise choice $k_\Lambda = 3\pi/(4R)$ to see the effect on density perturbations. The dimensionless power spectrum can be obtained by directly taking a scale derivative [106, 107],

$$\mathcal{P}_\delta(t, k) = \left. \frac{\partial \sigma_\delta^2(t, k')}{\partial \ln k'} \right|_{k' = \frac{4k}{3\pi}}, \quad (32)$$

where an abbreviation $\sigma_\delta^2(t; R \equiv 1/k) \equiv \sigma_\delta^2(t, k)$ as well as $\delta_{R \equiv 1/k}(t) \equiv \delta(t, k)$ is introduced for later clarity. This scale derivative on the density variance can be further transferred into scale derivatives of average values by

$$\frac{\partial \sigma_\delta^2(t, k)}{\partial \ln k} = \frac{\partial \langle \delta(t, k)^2 \rangle}{\partial \ln k} - 2 \langle \delta(t, k) \rangle \frac{\partial \langle \delta(t, k) \rangle}{\partial \ln k}, \quad (33)$$

where the scale derivative for the average value of an

arbitrary function of the density contrast reads

$$\frac{\partial \langle f(\delta(t, k)) \rangle}{\partial \ln k} = \int_{\bar{t}_i}^{U(\bar{t})} f(\delta(\bar{t}; \bar{t}')) e^{\beta \bar{t}'} \frac{\partial}{\partial \ln k} [\overline{PV}(\bar{t}', \bar{k})] d\bar{t}'. \quad (34)$$

Here we introduce $\overline{PV}(\bar{t}, \bar{k}) \equiv \overline{P}(\bar{t}, \bar{k}) \overline{V}(\bar{t}, \bar{k})$ for short with abbreviations $\overline{P}_{\bar{R} \equiv 1/\bar{k}}(\bar{t}) \equiv \overline{P}(\bar{t}, \bar{k})$ and $\overline{V}_{\bar{R} \equiv 1/\bar{k}}(\bar{t}) \equiv \overline{V}(\bar{t}, \bar{R})$. Therefore, we can numerically obtain the dimensionless power spectrum $\mathcal{P}_\delta(\bar{t}, \bar{k})$ for the accumulated overdensities from those delayed-decayed regions of any size and at any time, which can be specifically evaluated at a comoving scale that enters the Hubble horizon around the bubble percolation time, $\mathcal{P}_\delta(\bar{t}_*, \bar{k}_{H_*})$, as shown in dots in the bottom row of Fig. 7 with respect to the strength factor α_* and inverse duration $(\beta/H)_*$ for some fixed values of $(\beta/H)_*$ and α_* in the left and right panels, respectively. For a small $(\beta/H)_*$, $\mathcal{P}_\delta(\bar{t}_*, \bar{k}_{H_*})$ is almost quadratic in α_* but gradually deviates from that for a larger $(\beta/H)_*$. For a small α_* , $\mathcal{P}_\delta(\bar{t}_*, \bar{k}_{H_*})$ aligns closely with a complementary error function in $(\beta/H)_*$ but also slowly deviates from that for a larger α_* at the large $(\beta/H)_*$ limit, which should be asymptotic to $(\beta/H)_*^{-5}$ as theoretically anticipated. For the parameter space we explore in this study, we found a good fitting formula as

$$\mathcal{P}_\delta(\bar{t}_*, \bar{k}_{H_*}) = A(\alpha_*) \text{Erfc}[B(\alpha_*) (\beta/H)_* + C(\alpha_*)] \quad (35)$$

with $A(\alpha_*) = (0.00369\alpha_* + 0.0185)^2 \alpha_*^2$, $B(\alpha_*) = 0.00665\alpha_* + 0.0571$, and $C(\alpha_*) = 0.278\alpha_*^{0.615} + 0.436$, whose sole dependence on α_* and $(\beta/H)_*$ can be shown separately as solid curves in the left and right panels of the bottom row of Fig. 7, respectively, while the full dependence on both α_* and $(\beta/H)_*$ is presented in the top panel of Fig. 8 with the fitting formula shown in dashed curves.

At last, we are able to compute the power spectrum for the induced curvature perturbations from the previously obtained power spectrum of accumulated overdensities. Since the density perturbations $\delta(t, k)$ can be related to the induced curvature perturbations $\mathcal{R}(t, k) \equiv \mathcal{T}(t, k) \mathcal{R}(k)$ by [108]

$$\delta(t, k) = \frac{2(1+w)}{5+3w} \left(\frac{k}{a(t)H(t)} \right)^2 \mathcal{T}(t, k) \mathcal{R}(k) \quad (36)$$

in the radiation-dominated era with the equation of state parameter $w = 1/3$ where the transfer function admits $\mathcal{T}(t, k) = 3(\sqrt{3}aH/k)j_1(k/(\sqrt{3}aH))$, the corresponding power spectra can be related as

$$\mathcal{P}_\delta(t, k) = \frac{16}{3} \left(\frac{k}{aH} \right)^2 j_1 \left(\frac{k}{\sqrt{3}aH} \right)^2 \mathcal{P}_\mathcal{R}(k), \quad (37)$$

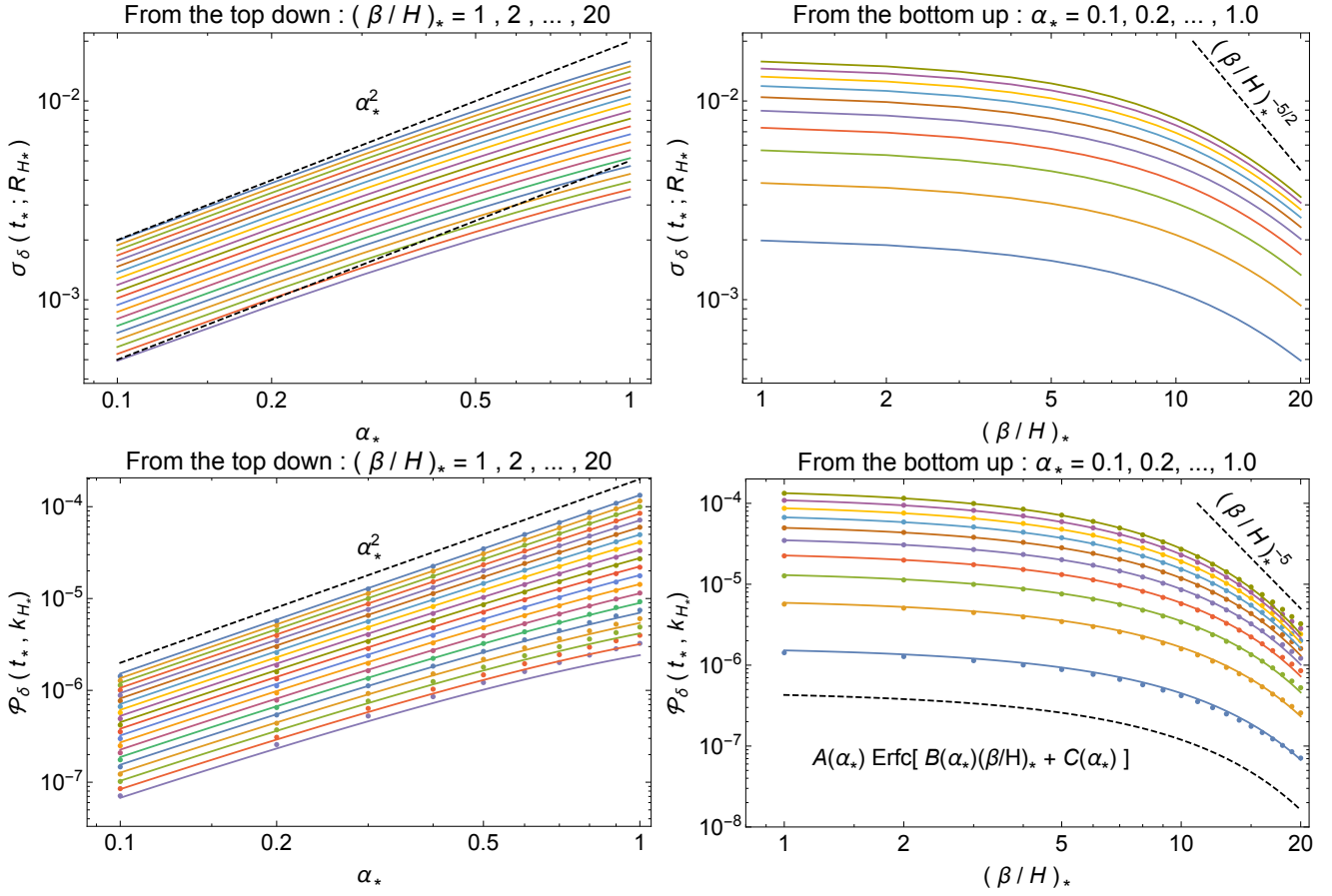


FIG. 7. The standard deviation (top) and dimensionless power spectrum (bottom) for the accumulated overdensity perturbations filtered at a scale that enters the Hubble horizon around the bubble percolation time. The parameter dependences are shown separately with respect to the strength factor α_* (left) and inverse duration $(\beta/H)_*$ (right) for some fixed values of $(\beta/H)_*$ and α_* , respectively.

whose value at horizon crossing simply reads

$$\mathcal{P}_{\mathcal{R}}(k_H) = \frac{3\mathcal{P}_{\delta}(t_{RH}, k_H)}{16j_1(1/\sqrt{3})^2}. \quad (38)$$

A useful numeric trick for this special value of the spherical Bessel function $j_1(1/\sqrt{3}) \approx 3/16$ serves as a good approximation with better than 1% accuracy. Therefore, the final dimensionless power spectrum of curvature perturbations induced by accumulated overdensities from delayed-decayed patches can be estimated as

$$\mathcal{P}_{\mathcal{R}}(k_{H_*}) \approx \frac{16}{3}\mathcal{P}_{\delta}(t_*, k_{H_*}) \quad (39)$$

at a comoving scale entering the Hubble horizon around the bubble percolations. However, the previously obtained numerical result for $\mathcal{P}_{\delta}(\bar{t}_*, \bar{k}_{H_*})$ shown in the top panel of Fig. 8 behaves as a function of the strength factor α_* and inverse duration $(\beta/H)_*$, while both dimensionless time \bar{t}_* and the dimensionless scale \bar{k}_{H_*} also depend on α_* and $(\beta/H)_*$, so does their ratio $\bar{k}_{H_*}/\sqrt{\bar{t}_*}$ as shown in black contours. In fact, this ratio can be directly re-

lated to the dimensional comoving scale k_{H_*} via the percolation temperature T_* as

$$k_{H_*} \equiv \bar{k}_{H_*} (C_0 \Gamma_0^{1/8}) = \frac{\bar{k}_{H_*}}{\sqrt{\bar{t}_*}} \left(\frac{g_{s0}}{g_{s*}} \right)^{\frac{1}{3}} \frac{\Gamma_0^{1/4}/M_{\text{Pl}}}{T_*/M_{\text{Pl}}} T_0, \quad (40)$$

where we have inserted $C_0 = (T_0/T_*)(g_{s0}/g_{s*})^{1/3} t_*^{-1/2}$ from the entropy conservation $g_{s*} T_*^3 a(t_*)^3 = g_{s0} T_0^3 a_0^3$ with $a(T_*) = C_0 t_*^{1/2}$ in the radiation dominated era, and $T_0 = 2.73\text{K}$ and $g_{s0} = 3.94$ are the cosmic microwave background (CMB) temperature and the effective number of degrees of freedom in entropy at present day, respectively, while Γ_0/M_{Pl} factor can be evaluated with (19) given α_* , $(\beta/H)_*$, and T_* . Therefore, for given percolation temperature T_* , the dimensionless comoving scale k_{H_*} can be mapped onto the same $\alpha_* - (\beta/H)_*$ plane where $\mathcal{P}_{\delta}(\bar{t}_*, \bar{k}_{H_*})$ is calculated. Now, we can draw various observational exclusion curves for $\mathcal{P}_{\mathcal{R}}(k)$ within the range of scales of observations. For example, in the bottom panels of Fig. 8, we have located two illustrative ranges of percolation temperatures so that the inferred comoving scale k_{H_*} within the $\alpha_* - (\beta/H)_*$ pa-

parameter space considered could cover the corresponding observational ranges where the observational constraints on the upper bound of $\mathcal{P}_{\mathcal{R}}(k)$ are imposed, that is, the CMB spectral y -distortion and μ -distortion constraints on $\mathcal{P}_{\mathcal{R}}(k) \lesssim 10^{-4}$ in the range $1 \text{ Mpc}^{-1} \lesssim k \lesssim 10^4 \text{ Mpc}^{-1}$ [109–111] and the ultra-compact minihalo (UCMH) abundance constraint $\mathcal{P}_{\mathcal{R}}(k) \lesssim 10^{-6}$ in the range $4 \times 10^3 \text{ Mpc}^{-1} \lesssim k \lesssim 4 \times 10^5 \text{ Mpc}^{-1}$ [112, 113]. Note that the current constraints on low-scale FOPTs from the above two observational bounds are slightly weaker than what we have obtained in our previous study [72], which could be traced back to different window functions. More carefully investigations are certainly needed in future for curvature-perturbation constraints on these low-scale FOPTs.

VI. CONCLUSIONS AND DISCUSSIONS

The interplay between the cosmological FOPTs and PBHs is of great interest to recent studies, among which the renewed attention on producing PBHs and curvature perturbations from cosmological FOPTs has been in hot debate. In this paper, we have revisited and elaborated our previously proposed accumulating mechanism for the overdensities produced in the delayed-decayed false vacuum island regions during the asynchronous progress of cosmological FOPTs. In particular, model-independent fitting formulas are given for future model-building investigations. Nevertheless, the current treatments are still far from satisfaction, which can be further improved in future studies from the following considerations:

First, numerical simulations are still needed to eventually settle the debates on whether the delayed-decayed regions could really lead to local overdensities, and whether these local overdensities could eventually collapse into PBHs according to the usual critical collapse criteria, and if not, whether they could eventually source curvature perturbations. The difficulty in carrying out such numerical simulations lies in the ultra-low probability of locating such delayed-decayed patches, requiring extremely large (and hence expensive) simulation volume to actually emerge such regions.

Second, if the first issue can be resolved and confirmed, the next challenge comes from analytically modeling the inhomogeneous evolution in completing the FOPT. Not only the full equations of motions are coupled integro-differential equations if the global background evolution is presumed *a priori*, but also the definition of overdensity relies on the averaged density over all possible nucleation histories that in turn requires the solved evolution of overdensities. In this study, we simply adopt a brute strategy to approximate the global background as in the radiation-dominated era and the averaged background as those patches with the earliest possible nucleation time since they greatly outnumber the others. Future investigations should be rigorously implemented either with iterative method [68] or transforming the two-

dimensional system of integro-differential equation into a seven-dimensional system of first-order ordinary differential equations [69].

Third, if the above two issues can both be resolved, then the PBH mass function and induced curvature perturbations are straightforward to calculate with our proposals. The final task is to find model-independent fitting formulas for different types of cosmological FOPTs with nucleation rates of constant and Dirac-delta forms as well as exponentially linear or quadratic in time.

Last, although our mechanism for producing PBHs and density perturbations is independent of details of particle physics models, the precise calculations, however, do rely on the underlying phase transition models. For example, the bubble wall velocity in the comoving radius of true vacuum bubbles from computing the false vacuum fraction has been fixed to be the speed of light. Lower wall velocity would further delay the percolation time and hence allow for later delayed-decayed nucleation time of the first bubble in those Hubble patches that collapse into smaller PBHs at an earlier time with higher abundances as shown qualitatively in Ref. [56]. Model dependency would further come into play if one further takes into account the full time evolution of the wall velocity $v_w(t)$ before reaching its terminal value [86] due to complex interactions between the bubble wall and thermal plasma. Another example is the strength factor of the phase transition defined as $\alpha(t) \equiv \Delta V(t)/\rho_r(t; t_i)$ usually evaluated at the percolation time where the vacuum energy density difference $\Delta V(T) \equiv V_+ - V_-(T)$ has been simply fixed at a constant value. In fact, for the slow FOPT with $1 \lesssim (\beta/H)_* \lesssim 20$ considered in this paper, the true vacuum potential energy density $V_-(T)$ could decrease significantly with decreasing temperature [88], enlarging the vacuum energy difference that accumulates over time in those delayed-decayed patches, whose overdensities would more rapidly saturate the PBH threshold with less delayed-decayed time, resulting in smaller PBH mass with larger abundance. We will leave these model dependencies in the time evolution of the bubble wall velocity $v_w(t)$ and true-vacuum energy density $V_-(T(t))$ in future work of specific particle physics models of cosmological FOPTs.

ACKNOWLEDGMENTS

We thank the helpful discussions with Ligong Bian, Jing Liu, Shi Pi, Misao Sasaki, Ke-Pan Xie, and the insightful correspondence with Yann Gouttenoire. This work is supported by the National Key Research and Development Program of China Grant No. 2021YFC2203004, No. 2021YFA0718304, and No. 2020YFC2201502, the National Natural Science Foundation of China Grants No. 12105344, No. 12235019, No. 11821505, No. 11991052, and No. 11947302, the Strategic Priority Research Program of the Chinese Academy of Sciences (CAS) Grant No. XDB23030100,

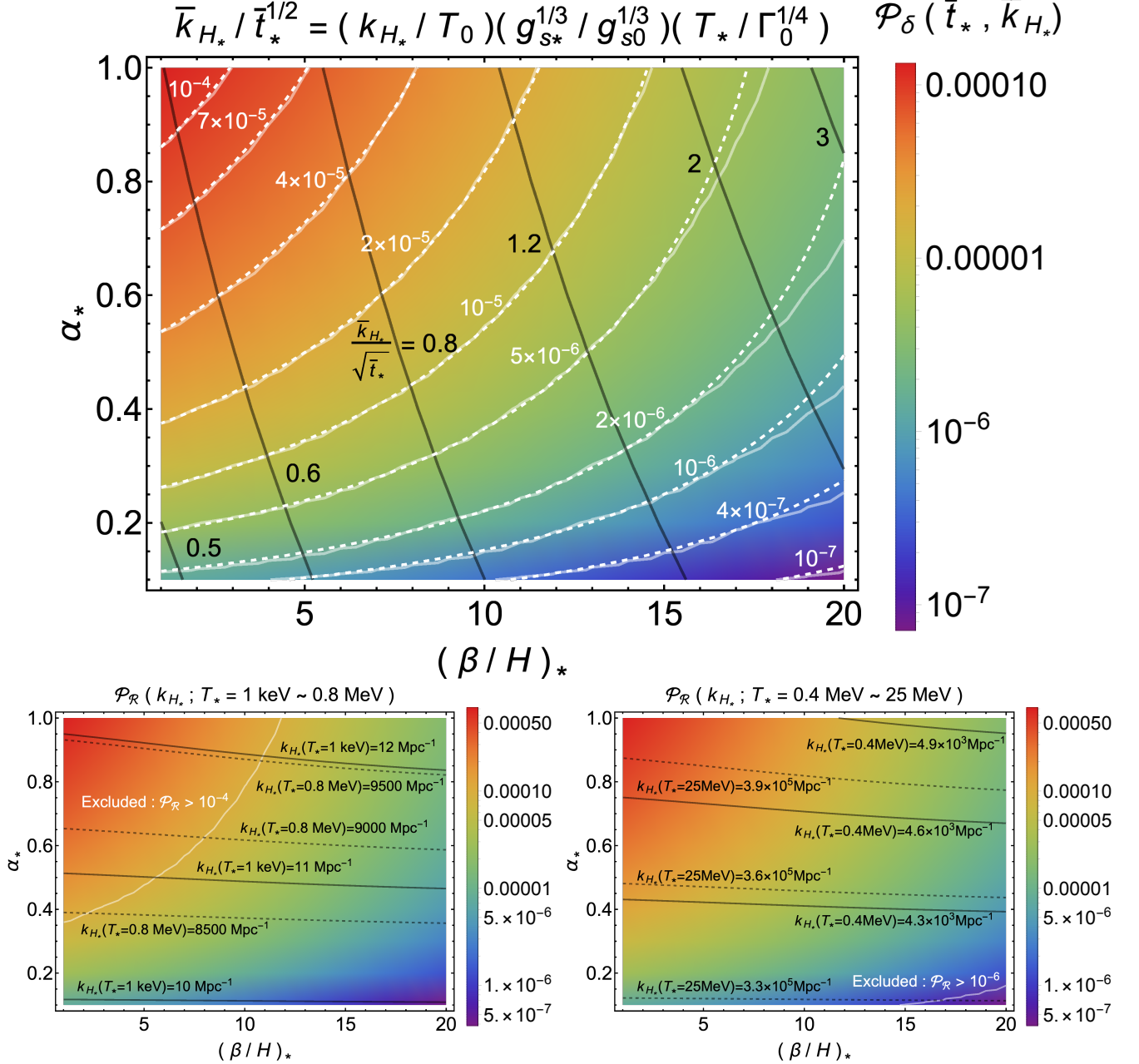


FIG. 8. The power spectra for the accumulated overdensities (top panel) with the fitting formula shown in white dashed contours and the induced curvature perturbations (bottom panels) with corresponding ranges of percolation temperatures to manifest the observational exclusion constraints (white contours).

No. XDA15020701, the Key Research Program of the CAS Grant No. XDPB15, the Key Research Program

of Frontier Sciences of CAS, and the Science Research Grants from the China Manned Space Project with No. CMS-CSST-2021-B01.

[1] Anupam Mazumdar and Graham White, “Review of cosmic phase transitions: their significance and ex-

perimental signatures,” Rept. Prog. Phys. **82**, 076901 (2019), arXiv:1811.01948 [hep-ph].

- [2] Mark B. Hindmarsh, Marvin Lüben, Johannes Lumma, and Martin Pauly, “Phase transitions in the early universe,” *SciPost Phys. Lect. Notes* **24**, 1 (2021), arXiv:2008.09136 [astro-ph.CO].
- [3] Robert Caldwell *et al.*, “Detection of early-universe gravitational-wave signatures and fundamental physics,” *Gen. Rel. Grav.* **54**, 156 (2022), arXiv:2203.07972 [gr-qc].
- [4] Peter Athron, Csaba Balázs, Andrew Fowlie, Lachlan Morris, and Lei Wu, “Cosmological phase transitions: From perturbative particle physics to gravitational waves,” *Prog. Part. Nucl. Phys.* **135**, 104094 (2024), arXiv:2305.02357 [hep-ph].
- [5] Rong-Gen Cai, Zhoujian Cao, Zong-Kuan Guo, Shao-Jiang Wang, and Tao Yang, “The Gravitational-Wave Physics,” *Natl. Sci. Rev.* **4**, 687–706 (2017), arXiv:1703.00187 [gr-qc].
- [6] Ligong Bian *et al.*, “The Gravitational-wave physics II: Progress,” *Sci. China Phys. Mech. Astron.* **64**, 120401 (2021), arXiv:2106.10235 [gr-qc].
- [7] Chiara Caprini *et al.*, “Science with the space-based interferometer eLISA. II: Gravitational waves from cosmological phase transitions,” *JCAP* **1604**, 001 (2016), arXiv:1512.06239 [astro-ph.CO].
- [8] Chiara Caprini *et al.*, “Detecting gravitational waves from cosmological phase transitions with LISA: an update,” *JCAP* **2003**, 024 (2020), arXiv:1910.13125 [astro-ph.CO].
- [9] Pierre Auclair *et al.* (LISA Cosmology Working Group), “Cosmology with the Laser Interferometer Space Antenna,” *Living Rev. Rel.* **26**, 5 (2023), arXiv:2204.05434 [astro-ph.CO].
- [10] M. Armano *et al.*, “Sub-Femto- g Free Fall for Space-Based Gravitational Wave Observatories: LISA Pathfinder Results,” *Phys. Rev. Lett.* **116**, 231101 (2016).
- [11] Pau Amaro-Seoane *et al.* (LISA), “Laser Interferometer Space Antenna,” (2017), arXiv:1702.00786 [astro-ph.IM].
- [12] Pau Amaro Seoane *et al.* (LISA), “Astrophysics with the Laser Interferometer Space Antenna,” *Living Rev. Rel.* **26**, 2 (2023), arXiv:2203.06016 [gr-qc].
- [13] Wen-Rui Hu and Yue-Liang Wu, “The Taiji Program in Space for gravitational wave physics and the nature of gravity,” *Natl. Sci. Rev.* **4**, 685–686 (2017).
- [14] Wen-Hong Ruan, Zong-Kuan Guo, Rong-Gen Cai, and Yuan-Zhong Zhang, “Taiji program: Gravitational-wave sources,” *Int. J. Mod. Phys. A* **35**, 2050075 (2020), arXiv:1807.09495 [gr-qc].
- [15] Yue-Liang Wu *et al.* (Taiji Scientific), “China’s first step towards probing the expanding universe and the nature of gravity using a space borne gravitational wave antenna,” *Commun. Phys.* **4**, 34 (2021).
- [16] Jun Luo *et al.* (TianQin), “TianQin: a space-borne gravitational wave detector,” *Class. Quant. Grav.* **33**, 035010 (2016), arXiv:1512.02076 [astro-ph.IM].
- [17] Jun Luo *et al.*, “The first round result from the TianQin-1 satellite,” *Class. Quant. Grav.* **37**, 185013 (2020), arXiv:2008.09534 [physics.ins-det].
- [18] Jianwei Mei *et al.* (TianQin), “The TianQin project: current progress on science and technology,” *PTEP* **2021**, 05A107 (2021), arXiv:2008.10332 [gr-qc].
- [19] Michael J. Baker, Moritz Breitbach, Joachim Kopp, and Lukas Mittnacht, “Primordial Black Holes from First-Order Cosmological Phase Transitions,” (2021), arXiv:2105.07481 [astro-ph.CO].
- [20] Kiyoharu Kawana and Ke-Pan Xie, “Primordial black holes from a cosmic phase transition: The collapse of Fermi-balls,” *Phys. Lett. B* **824**, 136791 (2022), arXiv:2106.00111 [astro-ph.CO].
- [21] Jing Liu, Ligong Bian, Rong-Gen Cai, Zong-Kuan Guo, and Shao-Jiang Wang, “Primordial black hole production during first-order phase transitions,” *Phys. Rev. D* **105**, L021303 (2022), arXiv:2106.05637 [astro-ph.CO].
- [22] S. W. Hawking, I. G. Moss, and J. M. Stewart, “Bubble Collisions in the Very Early Universe,” *Phys. Rev.* **D26**, 2681 (1982).
- [23] Matt Crawford and David N. Schramm, “Spontaneous Generation of Density Perturbations in the Early Universe,” *Nature* **298**, 538–540 (1982).
- [24] Ian G. Moss, “Black hole formation from colliding bubbles,” (1994), arXiv:gr-qc/9405045.
- [25] I. G. Moss, “Singularity formation from colliding bubbles,” *Phys. Rev.* **D50**, 676–681 (1994).
- [26] Ben Freivogel, Gary T. Horowitz, and Stephen Shenker, “Colliding with a crunching bubble,” *JHEP* **05**, 090 (2007), arXiv:hep-th/0703146.
- [27] Matthew C. Johnson, Hiranya V. Peiris, and Luis Lehner, “Determining the outcome of cosmic bubble collisions in full General Relativity,” *Phys. Rev. D* **85**, 083516 (2012), arXiv:1112.4487 [hep-th].
- [28] Alexander Kusenko, Misao Sasaki, Sunao Sugiyama, Masahiro Takada, Volodymyr Takhistov, and Edoardo Vitagliano, “Exploring Primordial Black Holes from the Multiverse with Optical Telescopes,” *Phys. Rev. Lett.* **125**, 181304 (2020), arXiv:2001.09160 [astro-ph.CO].
- [29] Tae Hyun Jung and Takemichi Okui, “Primordial black holes from bubble collisions during a first-order phase transition,” (2021), arXiv:2110.04271 [hep-ph].
- [30] Michael J. Baker, Joachim Kopp, and Andrew J. Long, “Filtered Dark Matter at a First Order Phase Transition,” *Phys. Rev. Lett.* **125**, 151102 (2020), arXiv:1912.02830 [hep-ph].
- [31] Jeong-Pyong Hong, Sunghoon Jung, and Ke-Pan Xie, “Fermi-ball dark matter from a first-order phase transition,” *Phys. Rev.* **D102**, 075028 (2020), arXiv:2008.04430 [hep-ph].
- [32] Jason Arakawa, Arvind Rajaraman, and Tim M. P. Tait, “Annihilogenesis,” *JHEP* **08**, 078 (2022), arXiv:2109.13941 [hep-ph].
- [33] Michael J. Baker, Moritz Breitbach, Joachim Kopp, Lukas Mittnacht, and Yotam Soreq, “Filtered baryogenesis,” *JHEP* **08**, 010 (2022), arXiv:2112.08987 [hep-ph].
- [34] Peisi Huang and Ke-Pan Xie, “Leptogenesis triggered by a first-order phase transition,” *JHEP* **09**, 052 (2022), arXiv:2206.04691 [hep-ph].
- [35] Michael J. Baker, Moritz Breitbach, Joachim Kopp, and Lukas Mittnacht, “Detailed Calculation of Primordial Black Hole Formation During First-Order Cosmological Phase Transitions,” (2021), arXiv:2110.00005 [astro-ph.CO].
- [36] James M. Cline, Benoit Laurent, Stuart Raby, and Jean-Samuel Roux, “PeV-scale leptogenesis, gravitational waves, and black holes from a SUSY-breaking phase transition,” *Phys. Rev. D* **107**, 095011 (2023), arXiv:2211.00422 [hep-ph].
- [37] Philip Lu, Kiyoharu Kawana, and Ke-Pan Xie, “Old

- phase remnants in first-order phase transitions,” *Phys. Rev. D* **105**, 123503 (2022), arXiv:2202.03439 [astro-ph.CO].
- [38] Kiyoharu Kawana, Philip Lu, and Ke-Pan Xie, “First-order phase transition and fate of false vacuum remnants,” *JCAP* **10**, 030 (2022), arXiv:2206.09923 [astro-ph.CO].
- [39] Peisi Huang and Ke-Pan Xie, “Primordial black holes from an electroweak phase transition,” *Phys. Rev. D* **105**, 115033 (2022), arXiv:2201.07243 [hep-ph].
- [40] Danny Marfatia and Po-Yan Tseng, “Correlated signals of first-order phase transitions and primordial black hole evaporation,” *JHEP* **08**, 001 (2022), [Erratum: *JHEP* **08**, 249 (2022)], arXiv:2112.14588 [hep-ph].
- [41] Po-Yan Tseng and Yu-Min Yeh, “511 keV line and primordial black holes from first-order phase transitions,” *JCAP* **08**, 035 (2023), arXiv:2209.01552 [hep-ph].
- [42] Thomas C. Gehrman, Barmak Shams Es Haghi, Kuvver Sinha, and Tao Xu, “The primordial black holes that disappeared: connections to dark matter and MHz-GHz gravitational Waves,” *JCAP* **10**, 001 (2023), arXiv:2304.09194 [hep-ph].
- [43] Ke-Pan Xie, “Pinning down the primordial black hole formation mechanism with gamma-rays and gravitational waves,” *JCAP* **06**, 008 (2023), arXiv:2301.02352 [astro-ph.CO].
- [44] Indra Kumar Banerjee and Ujjal Kumar Dey, “Probing the origin of primordial black holes through novel gravitational wave spectrum,” *JCAP* **07**, 024 (2023), arXiv:2305.07569 [gr-qc].
- [45] Pin-Jung Chen and Po-Yan Tseng, “Type Ia supernovae induced by primordial black holes from dark first-order phase transition,” *JHEAp* **39**, 106–113 (2023), arXiv:2305.14399 [astro-ph.HE].
- [46] Debasish Borah, Suruj Jyoti Das, and Indrajit Saha, “Dark matter from phase transition generated PBH evaporation with gravitational waves signatures,” (2024), arXiv:2401.12282 [hep-ph].
- [47] Marek Lewicki, Kristjan Mürsepp, Joosep Pata, Martin Vasar, Ville Vaskonen, and Hardi Veermäe, “Dynamics of false vacuum bubbles with trapped particles,” *Phys. Rev. D* **108**, 036023 (2023), arXiv:2305.07702 [hep-ph].
- [48] Katsuhiko Sato, Misao Sasaki, Hideo Kodama, and Kei-ichi Maeda, “Creation of Wormholes by First Order Phase Transition of a Vacuum in the Early Universe,” *Prog. Theor. Phys.* **65**, 1443 (1981).
- [49] Kei-ichi Maeda, Katsuhiko Sato, Misao Sasaki, and Hideo Kodama, “Creation of De Sitter-schwarzschild Wormholes by a Cosmological First Order Phase Transition,” *Phys. Lett. B* **108**, 98–102 (1982).
- [50] Katsuhiko Sato, Hideo Kodama, Misao Sasaki, and Kei-ichi Maeda, “Multiproduction of Universes by First Order Phase Transition of a Vacuum,” *Phys. Lett. B* **108**, 103–107 (1982).
- [51] Hideo Kodama, Misao Sasaki, Katsuhiko Sato, and Kei-ichi Maeda, “Fate of Wormholes Created by First Order Phase Transition in the Early Universe,” *Prog. Theor. Phys.* **66**, 2052 (1981).
- [52] K. Sato, “Production of Magnetized Black Holes and Wormholes by First Order Phase Transition in the Early Universe,” *Prog. Theor. Phys.* **66**, 2287–2290 (1981).
- [53] Hideo Kodama, Misao Sasaki, and Katsuhiko Sato, “Abundance of Primordial Holes Produced by Cosmological First Order Phase Transition,” *Prog. Theor. Phys.* **68**, 1979 (1982).
- [54] Angelo Caravano, Keisuke Inomata, and Sébastien Renaux-Petel, “The Inflationary Butterfly Effect: Non-Perturbative Dynamics From Small-Scale Features,” (2024), arXiv:2403.12811 [astro-ph.CO].
- [55] Song He, Li Li, Zhibin Li, and Shao-Jiang Wang, “Gravitational waves and primordial black hole productions from gluodynamics by holography,” *Sci. China Phys. Mech. Astron.* **67**, 240411 (2024), arXiv:2210.14094 [hep-ph].
- [56] Song He, Li Li, Sai Wang, and Shao-Jiang Wang, “Constraints on holographic QCD phase transitions from PTA observations,” (2023), arXiv:2308.07257 [hep-ph].
- [57] Yann Gouttenoire, “First-Order Phase Transition Interpretation of Pulsar Timing Array Signal Is Consistent with Solar-Mass Black Holes,” *Phys. Rev. Lett.* **131**, 171404 (2023), arXiv:2307.04239 [hep-ph].
- [58] Alberto Salvio, “Pulsar Timing Arrays and Primordial Black Holes from a Supercool Phase Transition,” (2023), arXiv:2312.04628 [hep-ph].
- [59] Katsuya Hashino, Shinya Kanemura, and Tomo Takahashi, “Primordial black holes as a probe of strongly first-order electroweak phase transition,” *Phys. Lett. B* **833**, 137261 (2022), arXiv:2111.13099 [hep-ph].
- [60] Katsuya Hashino, Shinya Kanemura, Tomo Takahashi, and Masanori Tanaka, “Probing first-order electroweak phase transition via primordial black holes in the effective field theory,” *Phys. Lett. B* **838**, 137688 (2023), arXiv:2211.16225 [hep-ph].
- [61] Alberto Salvio, “Supercooling in radiative symmetry breaking: theory extensions, gravitational wave detection and primordial black holes,” *JCAP* **12**, 046 (2023), arXiv:2307.04694 [hep-ph].
- [62] Yann Gouttenoire, “Primordial Black Holes from Conformal Higgs,” (2023), arXiv:2311.13640 [hep-ph].
- [63] Angela Conaci, Luigi Delle Rose, P. S. Bhupal Dev, and Anish Ghoshal, “Slaying Axion-Like Particles via Gravitational Waves and Primordial Black Holes from Supercooled Phase Transition,” (2024), arXiv:2401.09411 [astro-ph.CO].
- [64] Iason Baldes and María Olalla Olea-Romacho, “Primordial black holes as dark matter: interferometric tests of phase transition origin,” *JHEP* **01**, 133 (2024), arXiv:2307.11639 [hep-ph].
- [65] Kiyoharu Kawana, TaeHun Kim, and Philip Lu, “PBH formation from overdensities in delayed vacuum transitions,” *Phys. Rev. D* **108**, 103531 (2023), arXiv:2212.14037 [astro-ph.CO].
- [66] Yann Gouttenoire and Tomer Volansky, “Primordial Black Holes from Supercooled Phase Transitions,” (2023), arXiv:2305.04942 [hep-ph].
- [67] Marek Lewicki, Piotr Toczek, and Ville Vaskonen, “Primordial black holes from strong first-order phase transitions,” *JHEP* **09**, 092 (2023), arXiv:2305.04924 [astro-ph.CO].
- [68] Shinya Kanemura, Masanori Tanaka, and Ke-Pan Xie, “Primordial black holes from slow phase transitions: a model-building perspective,” (2024), arXiv:2404.00646 [hep-ph].
- [69] Marcos M. Flores, Alexander Kusenko, and Misao Sasaki, “Revisiting formation of primordial black holes in a supercooled first-order phase transition,” (2024), arXiv:2402.13341 [hep-ph].

- [70] Ryusuke Jinno, Jun'ya Kume, and Masaki Yamada, "Super-slow phase transition catalyzed by BHs and the birth of baby BHs," *Phys. Lett. B* **849**, 138465 (2024), arXiv:2310.06901 [hep-ph].
- [71] Koichiro Uehara, Albert Escrivà, Tomohiro Harada, Daiki Saito, and Chul-Moon Yoo, "Numerical simulation of type II primordial black hole formation," (2024), arXiv:2401.06329 [gr-qc].
- [72] Jing Liu, Ligong Bian, Rong-Gen Cai, Zong-Kuan Guo, and Shao-Jiang Wang, "Constraining First-Order Phase Transitions with Curvature Perturbations," *Phys. Rev. Lett.* **130**, 051001 (2023), arXiv:2208.14086 [astro-ph.CO].
- [73] Zhen-Min Zeng, Jing Liu, and Zong-Kuan Guo, "Enhanced curvature perturbations from spherical domain walls nucleated during inflation," *Phys. Rev. D* **108**, 063005 (2023), arXiv:2301.07230 [astro-ph.CO].
- [74] Zhen-Min Zeng and Zong-Kuan Guo, "Phase transition catalyzed by primordial black holes," (2024), arXiv:2402.09310 [astro-ph.CO].
- [75] Gilly Elor, Ryusuke Jinno, Soubhik Kumar, Robert McGehee, and Yuhsin Tsai, "Finite Bubble Statistics Constrain Late Cosmological Phase Transitions," (2023), arXiv:2311.16222 [hep-ph].
- [76] Matthew R. Buckley, Peizhi Du, Nicolas Fernandez, and Mitchell J. Weikert, "Dark Radiation Isocurvature from Cosmological Phase Transitions," (2024), arXiv:2402.13309 [hep-ph].
- [77] Marek Lewicki, Piotr Toczek, and Ville Vaskonen, "Black holes and gravitational waves from slow phase transitions," (2024), arXiv:2402.04158 [astro-ph.CO].
- [78] Sidney R. Coleman, "The Fate of the False Vacuum. 1. Semiclassical Theory," *Phys. Rev.* **D15**, 2929–2936 (1977), [Erratum: *Phys. Rev.* **D16**, 1248(1977)].
- [79] Curtis G. Callan, Jr. and Sidney R. Coleman, "The Fate of the False Vacuum. 2. First Quantum Corrections," *Phys. Rev.* **D16**, 1762–1768 (1977).
- [80] Andrei D. Linde, "Fate of the False Vacuum at Finite Temperature: Theory and Applications," *Phys. Lett.* **100B**, 37–40 (1981).
- [81] Andrei D. Linde, "Decay of the False Vacuum at Finite Temperature," *Nucl. Phys.* **B216**, 421 (1983), [Erratum: *Nucl. Phys.* **B223**, 544(1983)].
- [82] K. Enqvist, J. Ignatius, K. Kajantie, and K. Rummukainen, "Nucleation and bubble growth in a first order cosmological electroweak phase transition," *Phys. Rev.* **D45**, 3415–3428 (1992).
- [83] Mark Hindmarsh and Mulham Hijazi, "Gravitational waves from first order cosmological phase transitions in the Sound Shell Model," *JCAP* **1912**, 062 (2019), arXiv:1909.10040 [astro-ph.CO].
- [84] Alan H. Guth and Erick J. Weinberg, "Could the Universe Have Recovered from a Slow First Order Phase Transition?" *Nucl. Phys. B* **212**, 321–364 (1983).
- [85] Michael S. Turner, Erick J. Weinberg, and Lawrence M. Widrow, "Bubble nucleation in first order inflation and other cosmological phase transitions," *Phys. Rev.* **D46**, 2384–2403 (1992).
- [86] Rong-Gen Cai and Shao-Jiang Wang, "Effective picture of bubble expansion," *JCAP* **2021**, 096 (2021), arXiv:2011.11451 [astro-ph.CO].
- [87] Vinod K.S. Shante and Scott Kirkpatrick, "An introduction to percolation theory," *Advances in Physics* **20**, 325–357 (1971).
- [88] Rong-Gen Cai, Misao Sasaki, and Shao-Jiang Wang, "The gravitational waves from the first-order phase transition with a dimension-six operator," *JCAP* **1708**, 004 (2017), arXiv:1707.03001 [astro-ph.CO].
- [89] John Ellis, Marek Lewicki, and José Miguel No, "On the Maximal Strength of a First-Order Electroweak Phase Transition and its Gravitational Wave Signal," *JCAP* **04**, 003 (2019), arXiv:1809.08242 [hep-ph].
- [90] Ilia Musco, John C. Miller, and Luciano Rezzolla, "Computations of primordial black hole formation," *Class. Quant. Grav.* **22**, 1405–1424 (2005), arXiv:gr-qc/0412063.
- [91] Tomohiro Harada, Chul-Moon Yoo, and Kazunori Kohri, "Threshold of primordial black hole formation," *Phys. Rev. D* **88**, 084051 (2013), [Erratum: *Phys. Rev. D* **89**, 029903 (2014)], arXiv:1309.4201 [astro-ph.CO].
- [92] Bernard J. Carr, "The Primordial black hole mass spectrum," *Astrophys. J.* **201**, 1–19 (1975).
- [93] Bernard Carr and Florian Kuhnel, "Primordial Black Holes as Dark Matter: Recent Developments," *Ann. Rev. Nucl. Part. Sci.* **70**, 355–394 (2020), arXiv:2006.02838 [astro-ph.CO].
- [94] Gert Hütsi, Martti Raidal, Ville Vaskonen, and Hardi Veermäe, "Two populations of LIGO-Virgo black holes," *JCAP* **03**, 068 (2021), arXiv:2012.02786 [astro-ph.CO].
- [95] Alexander H. Nitz and Yi-Fan Wang, "Broad search for gravitational waves from subsolar-mass binaries through LIGO and Virgo's third observing run," *Phys. Rev. D* **106**, 023024 (2022), arXiv:2202.11024 [astro-ph.HE].
- [96] Zu-Cheng Chen, Chen Yuan, and Qing-Guo Huang, "Confronting the primordial black hole scenario with the gravitational-wave events detected by LIGO-Virgo," *Phys. Lett. B* **829**, 137040 (2022), arXiv:2108.11740 [astro-ph.CO].
- [97] Hiroko Niikura et al., "Microlensing constraints on primordial black holes with Subaru/HSC Andromeda observations," *Nature Astron.* **3**, 524–534 (2019), arXiv:1701.02151 [astro-ph.CO].
- [98] Hiroko Niikura, Masahiro Takada, Shuichiro Yokoyama, Takahiro Sumi, and Shogo Masaki, "Constraints on Earth-mass primordial black holes from OGLE 5-year microlensing events," *Phys. Rev. D* **99**, 083503 (2019), arXiv:1901.07120 [astro-ph.CO].
- [99] P. Mroz et al., "Microlensing optical depth and event rate toward the Large Magellanic Cloud based on 20 years of OGLE observations," (2024), arXiv:2403.02398 [astro-ph.GA].
- [100] P. Mroz et al., "No massive black holes in the Milky Way halo," (2024), arXiv:2403.02386 [astro-ph.GA].
- [101] Rong-Gen Cai, Tan Chen, Shao-Jiang Wang, and Xing-Yu Yang, "Gravitational microlensing by dressed primordial black holes," *JCAP* **03**, 043 (2023), arXiv:2210.02078 [astro-ph.CO].
- [102] Ewan D. Barr et al., "A pulsar in a binary with a compact object in the mass gap between neutron stars and black holes," *Science* **383**, 275–279 (2024), arXiv:2401.09872 [astro-ph.HE].
- [103] Zu-Cheng Chen and Lang Liu, "Is PSR J0514–4002E in a PBH-NS binary?" (2024), arXiv:2401.12889 [astro-ph.HE].
- [104] "Observation of Gravitational Waves from the Coalescence of a $2.5 - 4.5 M_{\odot}$ Compact Object and a Neutron Star," (2024), arXiv:2404.04248 [astro-ph.HE].

- [105] Qing-Guo Huang, Chen Yuan, Zu-Cheng Chen, and Lang Liu, “GW230529_181500: A Potential Primordial Binary Black Hole Merger in the Mass Gap,” (2024), arXiv:2404.05691 [gr-qc].
- [106] Rampei Kimura, Teruaki Suyama, Masahide Yamaguchi, and Ying-Li Zhang, “Reconstruction of Primordial Power Spectrum of curvature perturbation from the merger rate of Primordial Black Hole Binaries,” JCAP **04**, 031 (2021), arXiv:2102.05280 [astro-ph.CO].
- [107] Xinpeng Wang, Ying-li Zhang, Rampei Kimura, and Masahide Yamaguchi, “Reconstruction of power spectrum of primordial curvature perturbations on small scales from primordial black hole binaries scenario of LIGO/VIRGO detection,” Sci. China Phys. Mech. Astron. **66**, 260462 (2023), arXiv:2209.12911 [astro-ph.CO].
- [108] Amandeep S. Josan, Anne M. Green, and Karim A. Malik, “Generalised constraints on the curvature perturbation from primordial black holes,” Phys. Rev. D **79**, 103520 (2009), arXiv:0903.3184 [astro-ph.CO].
- [109] Jens Chluba, Adrienne L. Erickcek, and Ido Ben-Dayan, “Probing the inflaton: Small-scale power spectrum constraints from measurements of the CMB energy spectrum,” Astrophys. J. **758**, 76 (2012), arXiv:1203.2681 [astro-ph.CO].
- [110] Jens Chluba, Jan Hamann, and Subodh P. Patil, “Features and New Physical Scales in Primordial Observables: Theory and Observation,” Int. J. Mod. Phys. D **24**, 1530023 (2015), arXiv:1505.01834 [astro-ph.CO].
- [111] Matteo Lucca, Nils Schöneberg, Deanna C. Hooper, Julien Lesgourgues, and Jens Chluba, “The synergy between CMB spectral distortions and anisotropies,” JCAP **02**, 026 (2020), arXiv:1910.04619 [astro-ph.CO].
- [112] Hamish A. Clark, Geraint F. Lewis, and Pat Scott, “Investigating dark matter substructure with pulsar timing – I. Constraints on ultracompact minihaloes,” Mon. Not. Roy. Astron. Soc. **456**, 1394–1401 (2016), [Erratum: Mon.Not.Roy.Astron.Soc. 464, 2468 (2017)], arXiv:1509.02938 [astro-ph.CO].
- [113] Hamish A. Clark, Geraint F. Lewis, and Pat Scott, “Investigating dark matter substructure with pulsar timing – II. Improved limits on small-scale cosmology,” Mon. Not. Roy. Astron. Soc. **456**, 1402–1409 (2016), [Erratum: Mon.Not.Roy.Astron.Soc. 464, 955–956 (2017)], arXiv:1509.02941 [astro-ph.CO].